UNIVERSITY OF CALIFORNIA

Radiation Laboratory

BERKELEY, CALIFORNIA

DISCLAIMER

UNIVERSITY OF CALIFORNIA
RADIATION LABORATORY

Cover Sheet
Do not remove

UNCLASSIFIED

INDEX NO. UCRL-167
This document contains 26 pages
and 31 plates of figures.
This is copy 87 of 100 Series A
Issued to: UCRL Files

RESTRICTED
Classification

Each person who received this document must sign the cover sheet in the space below.

Route to	Noted by	Date	Route to	Noted by	Date

UCRL-167

Physics-General

UNIVERSITY OF CALIFORNIA

Radiation Laboratory

PHYSICS DIVISION

QUARTERLY REPORT MAY 1, 1948 TO AUGUST 1, 1948

August 19, 1948

Berkeley, California

UCRL-167
Physics-General
-2-

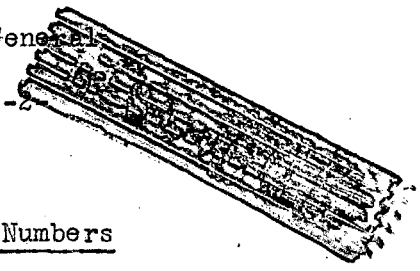

Standard Distribution	Copy Numbers
Argonne National Laboratory	1-8
Armed Forces Special Weapons Project	9
Atomic Energy Commission, Washington	10-11
Battelle Memorial Institute	12
Brookhaven National Laboratories	13-20
Carbide & Carbon Chemicals Corporation (K-25 Area)	21-24
Carbide & Carbon Chemicals Corporation (Y-12 Area)	25-28
Columbia University (Dunning)	29
General Electric Company	30-33
Hanford Directed Operations	34-38
Iowa State College	39
Los Alamos	40-42
Monsanto Chemical Company, Dayton	43-44
National Bureau of Standards	45-46
Naval Radiological Defense Laboratory	47
NEPA	48
New York Directed Operations	49-50
Oak Ridge National Laboratory	51-58
Patent Advisor, Washington	59
Technical Information Division, ORDO	60-74
UCLA Medical Research Division Laboratory, Warren	75
University of California Radiation Laboratory, Files	76-90
University of Rochester	91-92
Office of Chicago Directed Operations	93
Further Distribution, University of California Radiation Laboratory	
E. O. Lawrence	94
Patent Department	95
Chemistry Department	96
J. G. Hamilton	97
E. Segre	98
J. H. Lawrence	99
R. Ball	100
	100

Information Division
Radiation Laboratory
University of California
Berkeley, California

UNCLASSIFIED

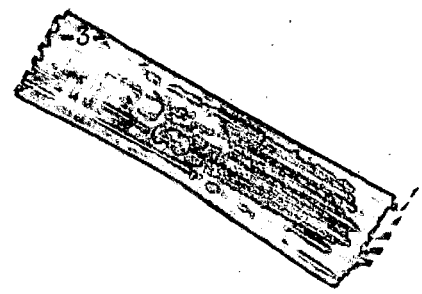

TABLE OF CONTENTS

I. GENERAL PHYSICS RESEARCH

1. Cloud Chamber Program

Evans Hayward

N-P Scattering

The cloud chamber group has completed the n-p scattering problem. The angular distribution of the protons elastically scattered by the neutrons from the 184-inch cyclotron has been measured. This distribution (Fig. 1) is based on 1760 knock-on proton tracks due to neutrons with energies greater than 40 Mev. Tracks that dipped down from the horizontal by more than 50° have been excluded because they are subject to large errors in measurement. The data have been multiplied by a geometrical weighting factor to correct for this omission. The standard deviations are based only on the number of tracks.

The conclusions to be drawn from this experiment are that the scattering is not isotropic in the center of mass system and that charge exchange is taking place because of the peak of protons in the forward direction.

Delayed Neutrons

When the elements immediately above oxygen in the periodic table are bombarded with 195 Mev deuterons, they yield delayed neutrons corresponding to a half-life of 4.14 $\pm$ 0.04 seconds.[1] The nucleus responsible for this period has been identified by Alvarez[2] to be N^{17}. N^{17} undergoes β-decay with the 4.14 sec period and the O^{17} nucleus which is formed emits the delayed neutron.

The energy spectrum of the delayed neutrons has been obtained by measuring the energies of their knock-on protons in a hydrogen-filled cloud chamber. Fig. 2 shows the geometry of the experiment. A LiF target was bombarded for about 30 sec in the deuteron beam and then blown out through a pneumatic tube to a location about 5 feet from the concrete shielding and 6 feet from the cloud chamber. About a second after the arrival of the target the cloud chamber was expanded manually. Since the cloud chamber clearing field is not shorted out until the time of the expansion, only those ions formed in the cloud chamber after the target stopped moving formed nuclei for droplets. The cyclotron was turned off after the bombardment and since it took about eight seconds for the target to get to its final position outside the concrete shielding, we may be quite certain that the neutrons observed at the cloud chamber originated at the target and not from the cyclotron.

The neutron energy is related to the energy of its knock-on proton by the relation $En = Ep/\cos^2\theta$, where θ is the scatter angle. The proton energies have been determined from the lengths of their tracks in the cloud chamber. The range-energy relation for the chamber pressure of H_2 saturated with a 2:1 alcohol-water mixture has been calculated by A. A. Garren (Fig. 3).

The proton ranges and the angle that the proton makes with the direction of the incident neutron have been measured by reprojection. Knock-on proton tracks that start in a region 9-3/4 x 7 x 4-1/2 inches have been measured. This is the maximum area that could be used and still have all the tracks that start within it also stop in the chamber.

The tracks have also been selected on the basis of their width. Only those

proton tracks due to neutrons that passed through the chamber before the expansion have been included. 0.1 cm was taken as the smallest acceptable width. No track that was so old that the negative and positive ions were separated into two columns was included. The ranges of the protons have been corrected for the diffusion of the ions by subtracting the width of the track, measured in a horizontal plane, from its length. The clearing field is vertical so that if the track is almost horizontal, the error introduced by the clearing field pulling the ions up or down is negligible. Only those protons scattered by neutrons having an energy greater than 0.46 Mev have been included.

The error in measuring the range of a proton is ± 10%, but since the average rate of energy loss $\frac{dE}{dX}$ is 0.1 $\frac{\text{Mev}}{\text{cm}}$ in this energy range, the error in the proton energy is about ± 1%. This error is very small compared to the error in measuring the angles. In order to minimize not only the errors in measuring the angles but also the errors due to the fact that the neutrons may have been scattered before producing a knock-on proton, protons with scatter angles greater than 30° have been excluded.

The measurements of the angles have been made carefully and are reproducible to ± 2°. About 50% of the knock-on protons exhibited small angle scattering in the gas before they reached the end of their range. If scattering occurred near the beginning of the track or was unobserved for some other reason, this would make an error of perhaps as much as ± 5° in the measurement of the scatter angle in some cases. We believe that all the cases of scattering in the gas have been found. Assuming that the neutron comes directly from the target, then the error in the energy due to the error in measuring the angle is $\frac{\Delta E}{E} = \pm 2 \tan \theta \Delta\theta$. The error for $\theta = 30^\circ$ and $\Delta\theta = 2^\circ$ is ± 4%.

Fig. 4 shows the energy spectrum of the knock-on protons and Fig. 5, that for the neutrons producing them. At first glance the neutrons energy distribution appears to be a line with energy about 1 Mev. The proton energy distribution, however, shows 12 tracks with energies greater than 1.2 Mev; these must come from neutrons with at least that energy regardless of their scatter angles. Fig. 6 shows the energy distribution of the neutrons if we assume that we are not measuring one energy and correct the distribution for the variation of the scattering cross-section with energy.

Mesons

Attempts were made to detect mesons in the re-entrant chamber of the cyclotron but the background was too high for practical cloud chamber operation.

---

[1] N. Knable, E. O. Lawrence, C. E. Leith, B. J. Moyer, and R. L. Thornton, Bul. Am. Phys. Soc. F9, April 29, 1948

[2] L. W. Alvarez, Bul. Am. Phys. Soc. F11, April 29, 1948

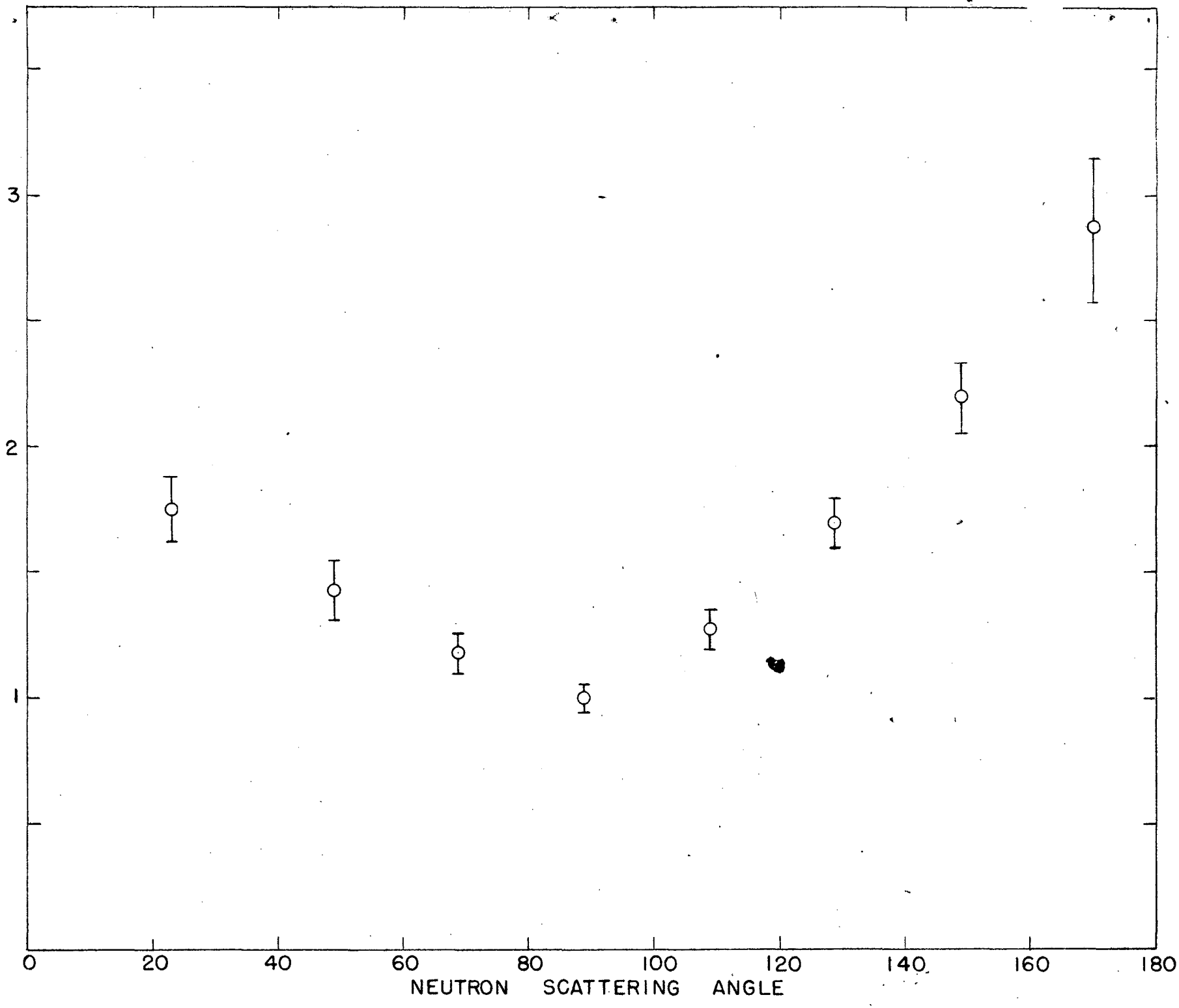
3
2
1
0
20
40
60
80
100
120
140
160
180
NEUTRON SCATTERING ANGLE

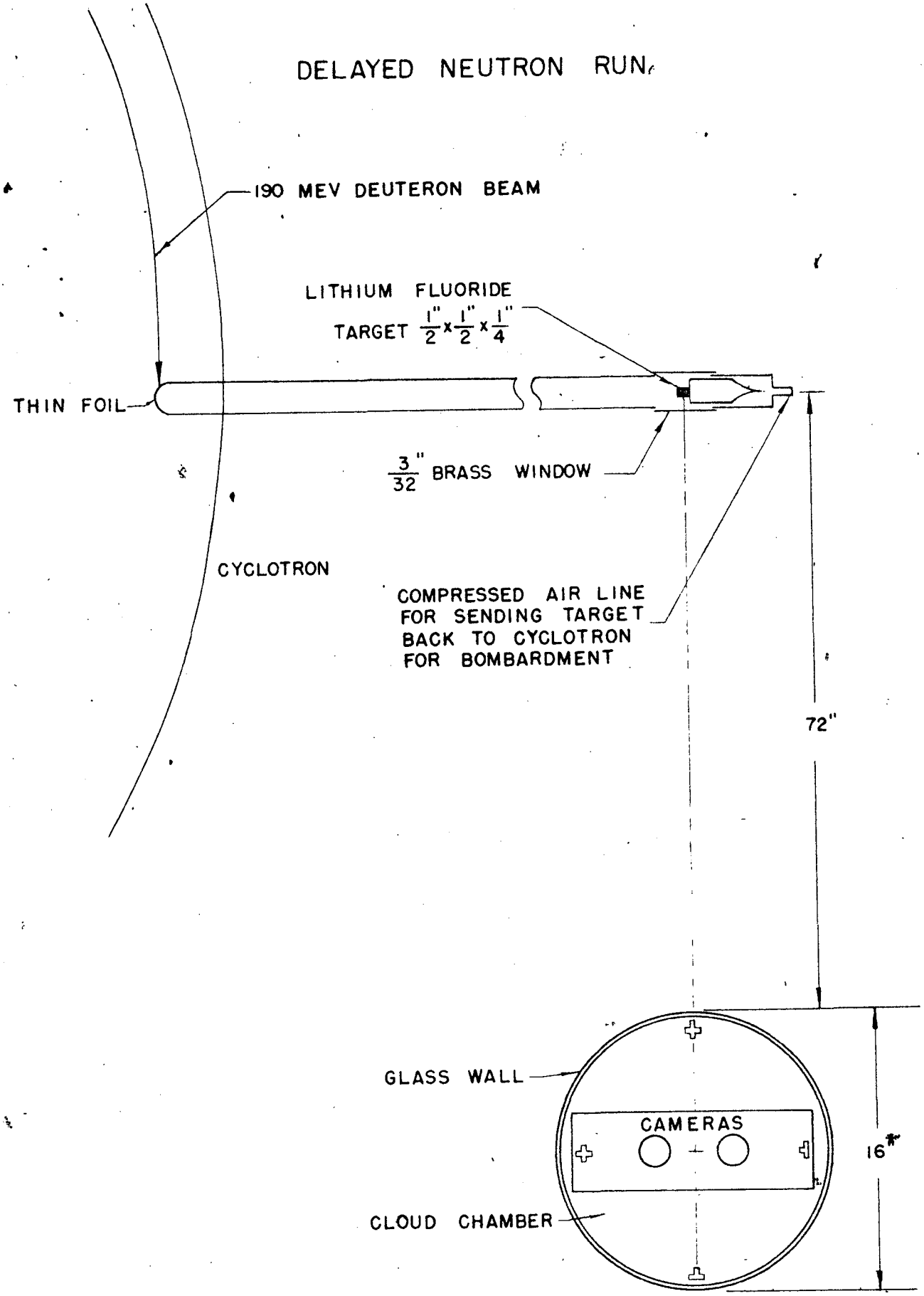
DELAYED NEUTRON RUN
190 MEV DEUTERON BEAM
LITHIUM FLUORIDE
TARGET 1" x 1" x 1"
2 2 4
THIN FOIL
3"
32
BRASS WINDOW
CYCLOTRON
COMPRESSED AIR LINE
FOR SENDING TARGET
BACK TO CYCLOTRON
FOR BOMBARDMENT
72"
GLASS WALL
CAMERAS
16"
CLOUD CHAMBER

FIG. 2

RANGE OF PROTONS IN HYDROGEN GAS, ALCOHOL AND WATER VAPOR AT A 2:1 RATIO BY VOLUME (OF THE LIQUID), AT 129.4 cm Hg AND 20° C

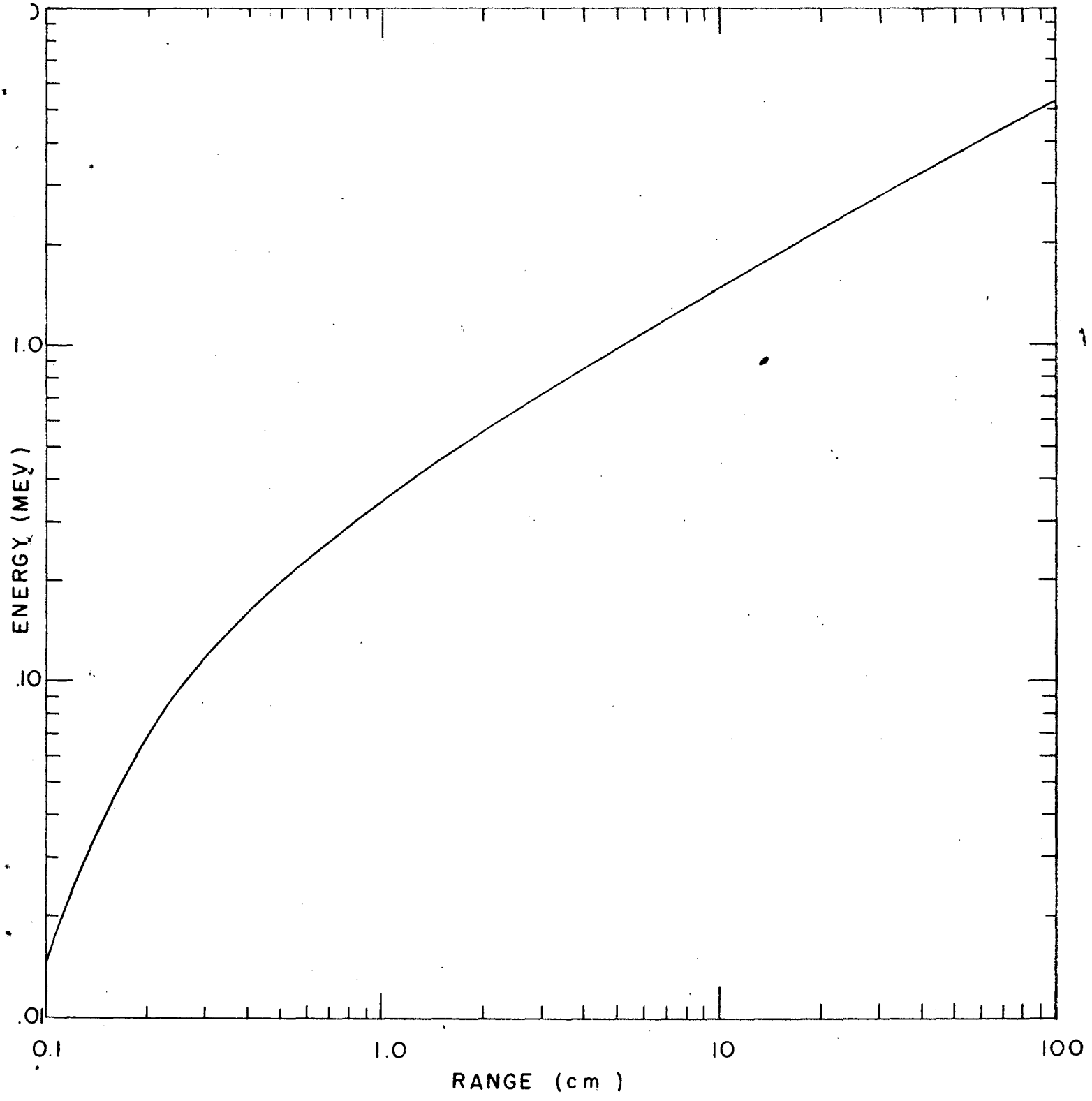

FIG. 3

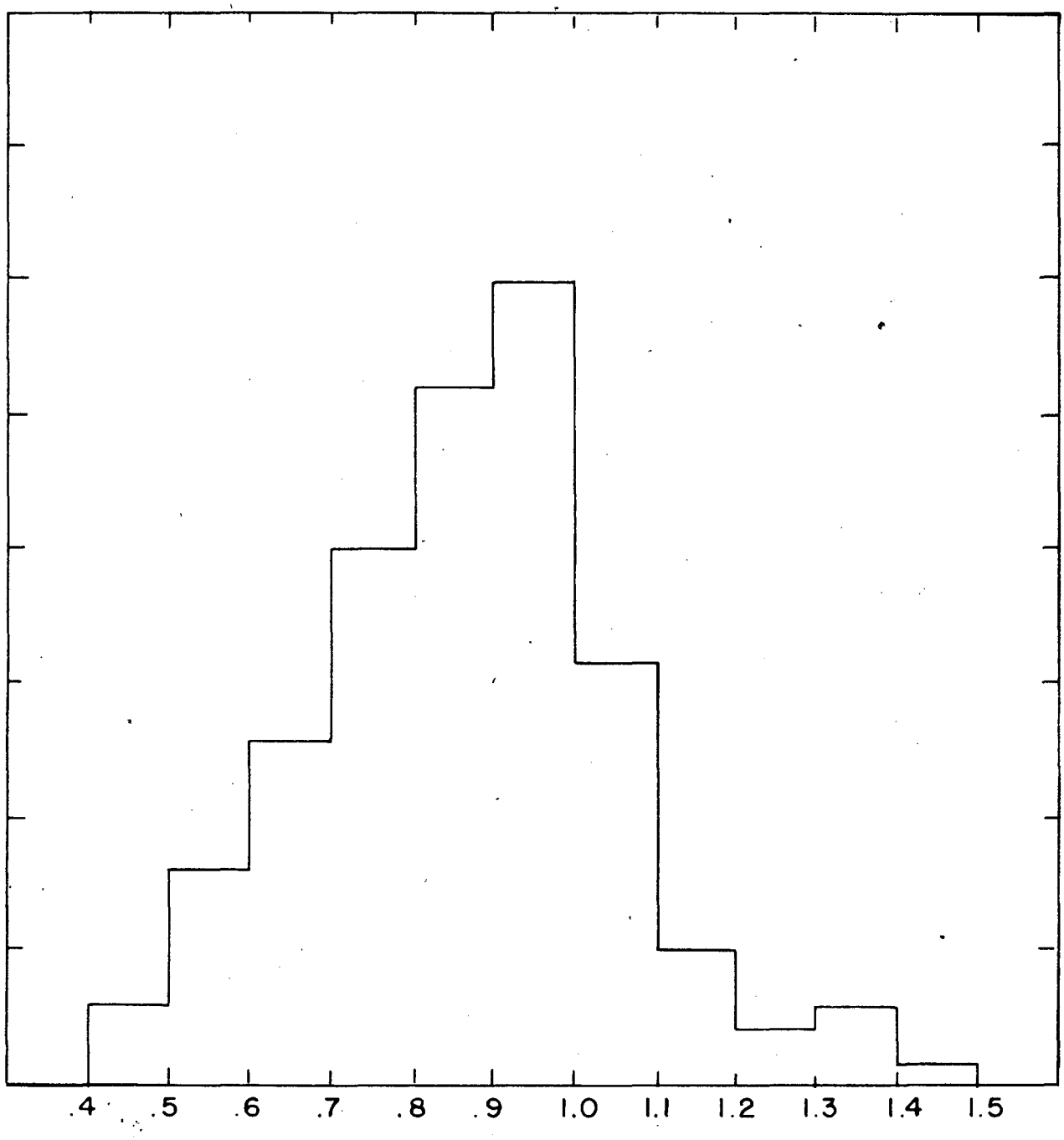

FIG. 4

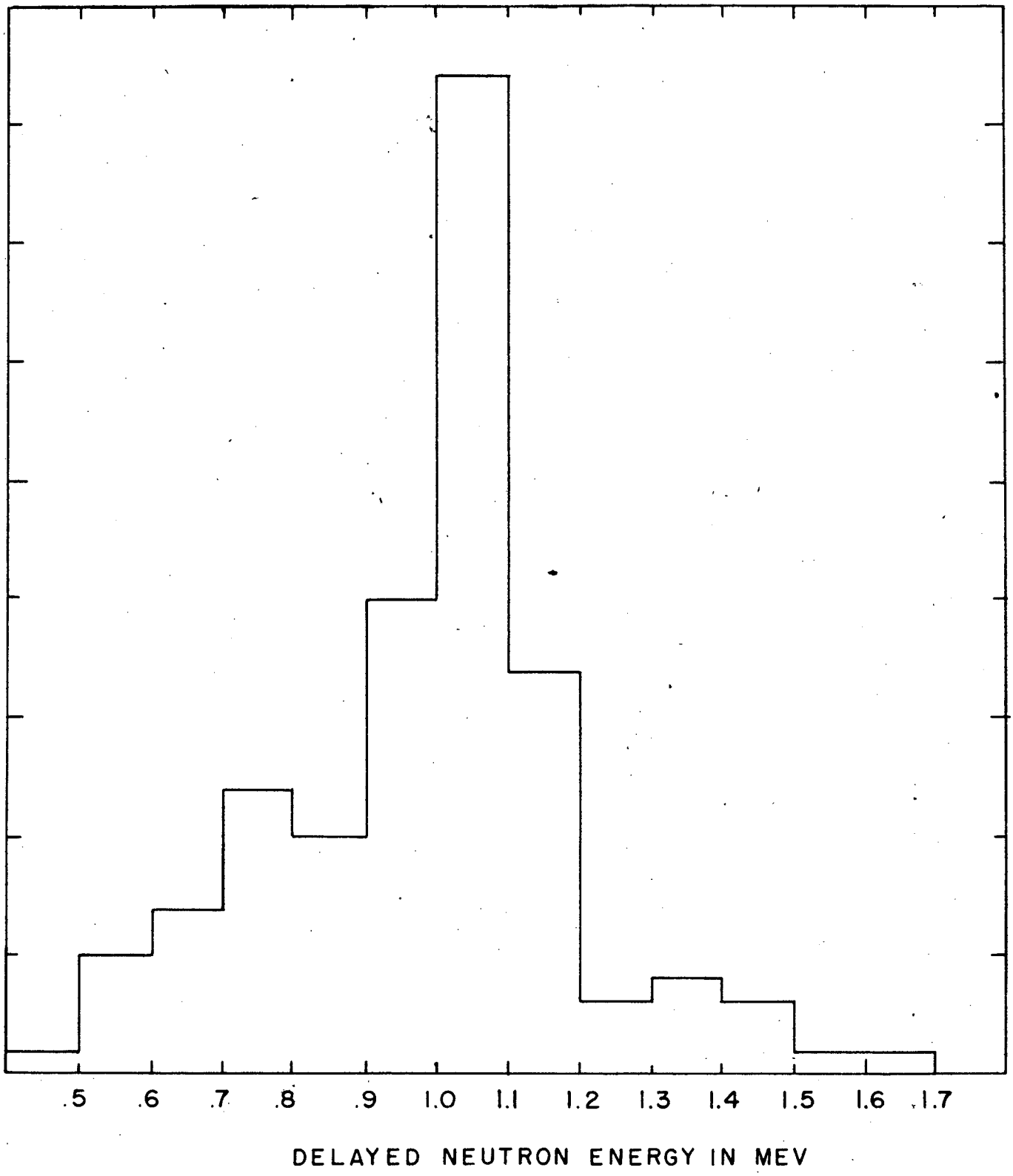

FIG. 5

12681-I

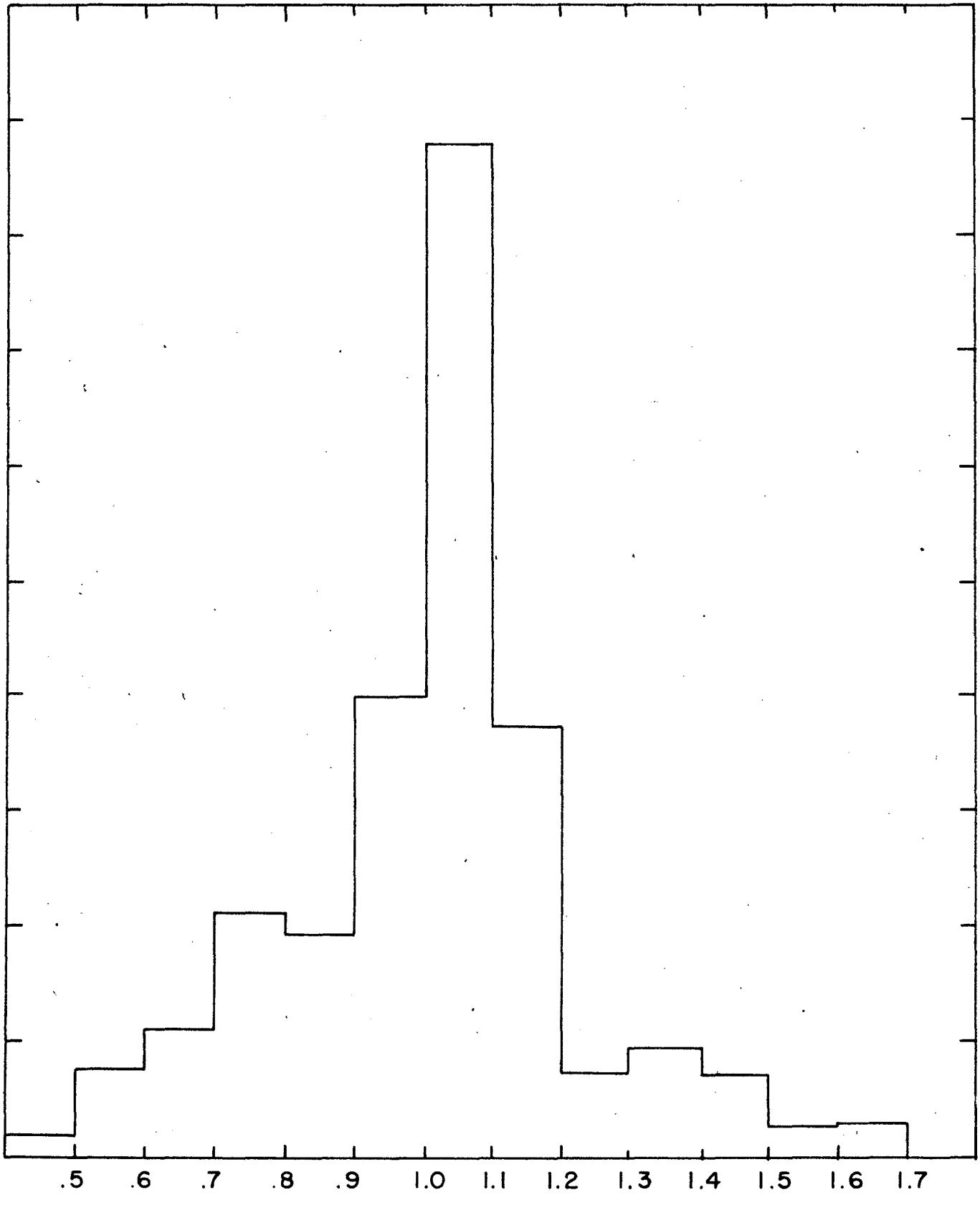

DELAYED NEUTRON ENERGY SPECTRUM
CORRECTED FOR N-P CROSS-SECTION

FIG. 6

12682-1

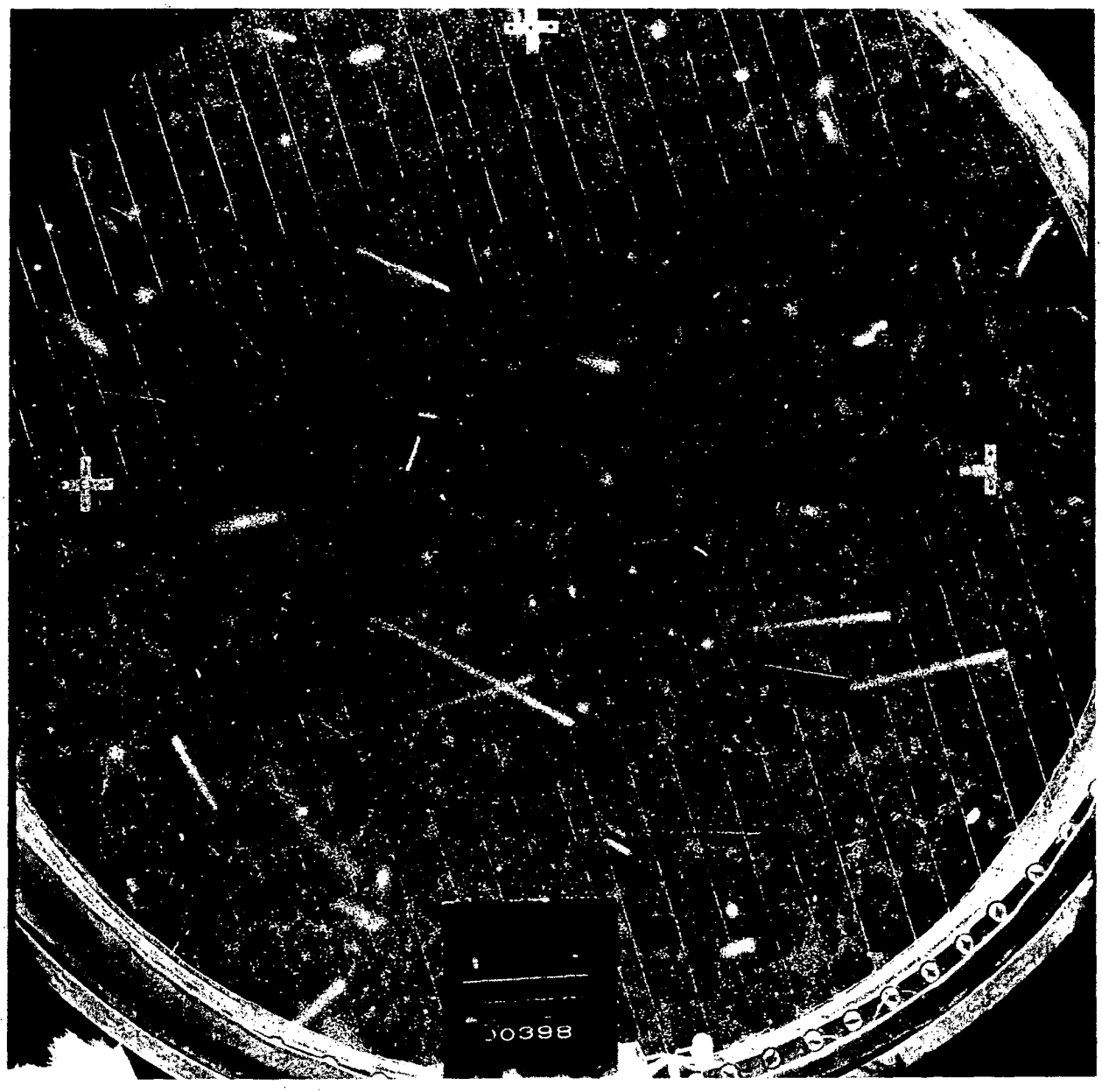

FIG. 7

EXAMPLE OF A PHOTOGRAPH SHOWING THE KNOCK-ON PROTONS AGAINST THE γ-RAY BACKGROUND

2. Film Program

Eugene Gardner

Observations on Tracks of Positive Mesons

The mesons first detected at the 184-inch Berkeley cyclotron were known to be negatively charged, since the apparatus was arranged so that negative but not positive particles from the target could reach the photographic plates. We have now detected positive mesons by placing plates in a position to receive positively charged particles from the target. As in the case of the exposures to negative mesons, the target was bombarded with alpha-particles of energy approximately 380 Mev. Ilford C.2 and C.3 plates and Eastman NTB plates, each of emulsion thickness about 100 microns, have been found to be suitable for this use. The exposures to positive mesons are more difficult than exposures to negative ones for two reasons: (1) Positive mesons which leave the target in the forward direction of the beam are deflected by the magnetic field back into the region of the circulating beam, as shown in Fig. 1. Any apparatus placed closer to the center of the cyclotron than the target must be designed in such a way that it does not cut off the circulating beam. (2) Protons and alpha-particles from the target can follow approximately the same trajectories as the positive mesons. These protons and alpha-particles contribute to the "background" of unwanted tracks on the plates.

Two methods of making exposures to positive mesons have been successful enough to enable us to make a study of the positive meson tracks. In the first method the plates to receive the positive mesons are placed below the circulating beam, as shown in Fig. 2. Mesons are received which leave the target moving at a small angle downward from the beam direction. Plates to receive negative mesons of about the same energy and angular range may be placed on the opposite side of the target as shown in the figure. Shielding is provided on the side from which the beam comes in order to prevent scattered beam particles from reaching the plates. For mesons which strike the plate at right angles to the edge, the energy range is about 2-5 Mev. For meson trajectories at other angles the energy at a given point on the plate is larger, so that the energy range of the mesons counted on the plates is not very well defined.

In a second method of detecting positive mesons, the photographic plates are placed in a position to receive mesons which leave the target in a direction opposite to the beam direction. The arrangement is shown in Fig. 3. Plates exposed in this way have tracks of negative msons along one edge, and tracks of positive mesons along the opposite edge. In this method, as in the preceding one, the energy range of the mesons received by the plates is not well defined.

Methods of detecting positive mesons in which the plates are placed at the 270° or 360° position have been tried, but they did not seem to be as good as the methods described above.

The appearance of the positive meson tracks under the microscope is similar to that of negative meson tracks: they have a characteristic grain density change along the track and a characteristic bending associated with small-angle scattering. A measurement of the masses of the mesons can be obtained by measuring the bending in the magnetic field of the cyclotron and the range in the emulsion. The radius of curvature of the meson's trajectory from the target to the plate is calculated from the position on the plate at which the track is found, and the angle which the track makes with the edge of the plate. The mass determination has not yet been made with any precision; however, preliminary measurements indicate that there are two groups of mesons having masses of about 300 and 200 electronic masses respectively. It is presumed that they are the same as the π and

μ mesons described by Lattes, Occhialini and Powell (Nature 160, 453, 486 (1947)). Neither the heavy nor the light positive mesons initiate stars. Most of the heavy positive mesons disintegrate to give observable secondary mesons. It is thought that all of the heavy positive mesons give secondaries, but that in some cases the secondaries are not seen. For all of the secondary mesons which stop in the emulsion the range is about 600 microns, corresponding to an energy of about 4 Mev. These observations of the heavy positive meson decay are in agreement with the $\pi - \mu$ decay described by Lattes, Occhialini, and Powell.

Examples of disintegration of heavy positive mesons into secondaries are shown in Figs. 4 and 5. Fig. 4 is taken from an Eastman NTB plate, and Fig. 5 is taken from an Ilford C.3 plate. In each case the heavy positive meson enters from the bottom left and slows down and stops. At the point at which the heavy positive meson stops a secondary meson is initiated, moving toward the right.

By means of symmetrically placed plates as shown in Fig. 2, we have measured the relative numbers of positive and negative mesons. The energy range studied is not as large as that accepted by the plates, but includes roughly energies from 2 to 3 Mev. In this energy range 40 positive mesons have been counted as compared with 136 negative ones in an equivalent area. Of the 40 positive mesons, 26 are known to be heavy since they form observable secondaries. Some of the secondaries may have been missed, so that the number of heavy mesons may be larger than 26. Most of the 136 negative mesons are heavy.

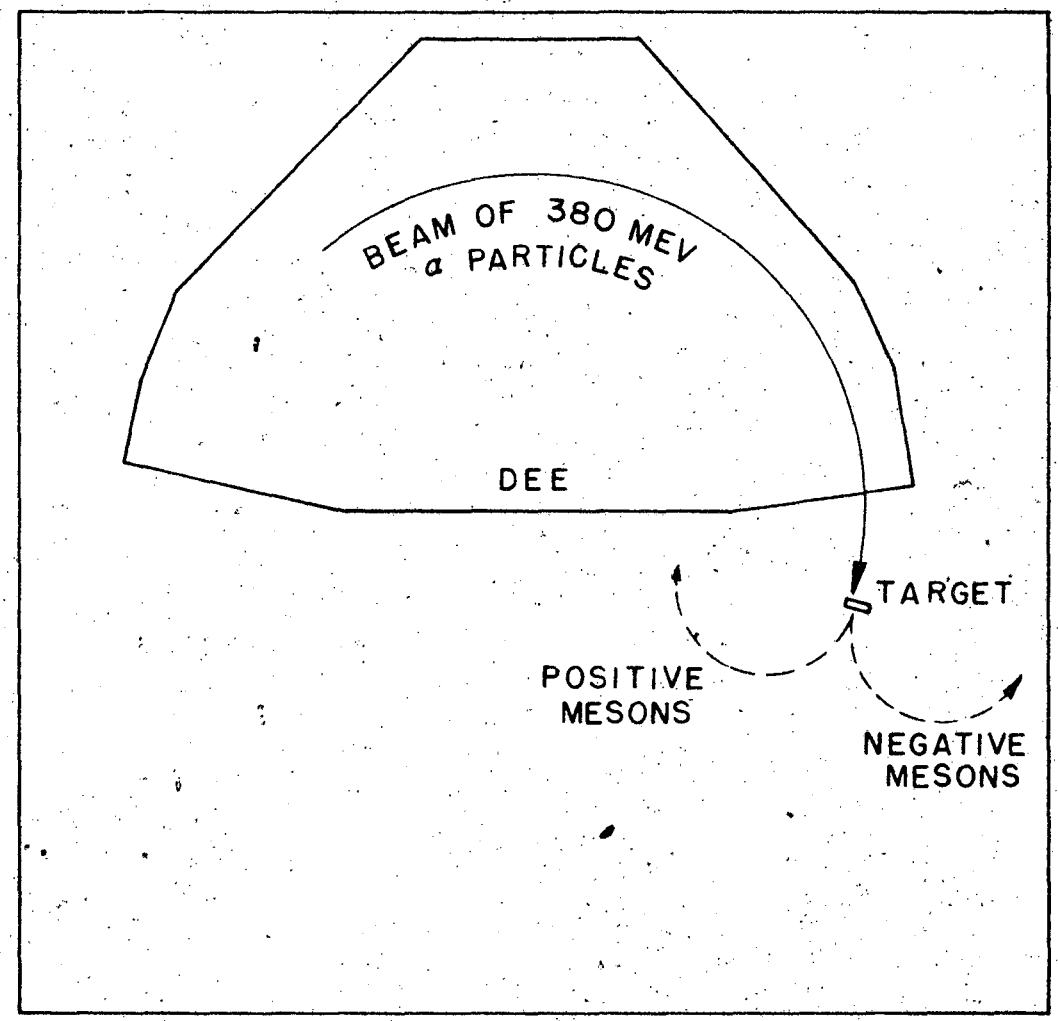

PLAN VIEW OF CYCLOTRON

0 1 2 3
FEET

FIG. 1

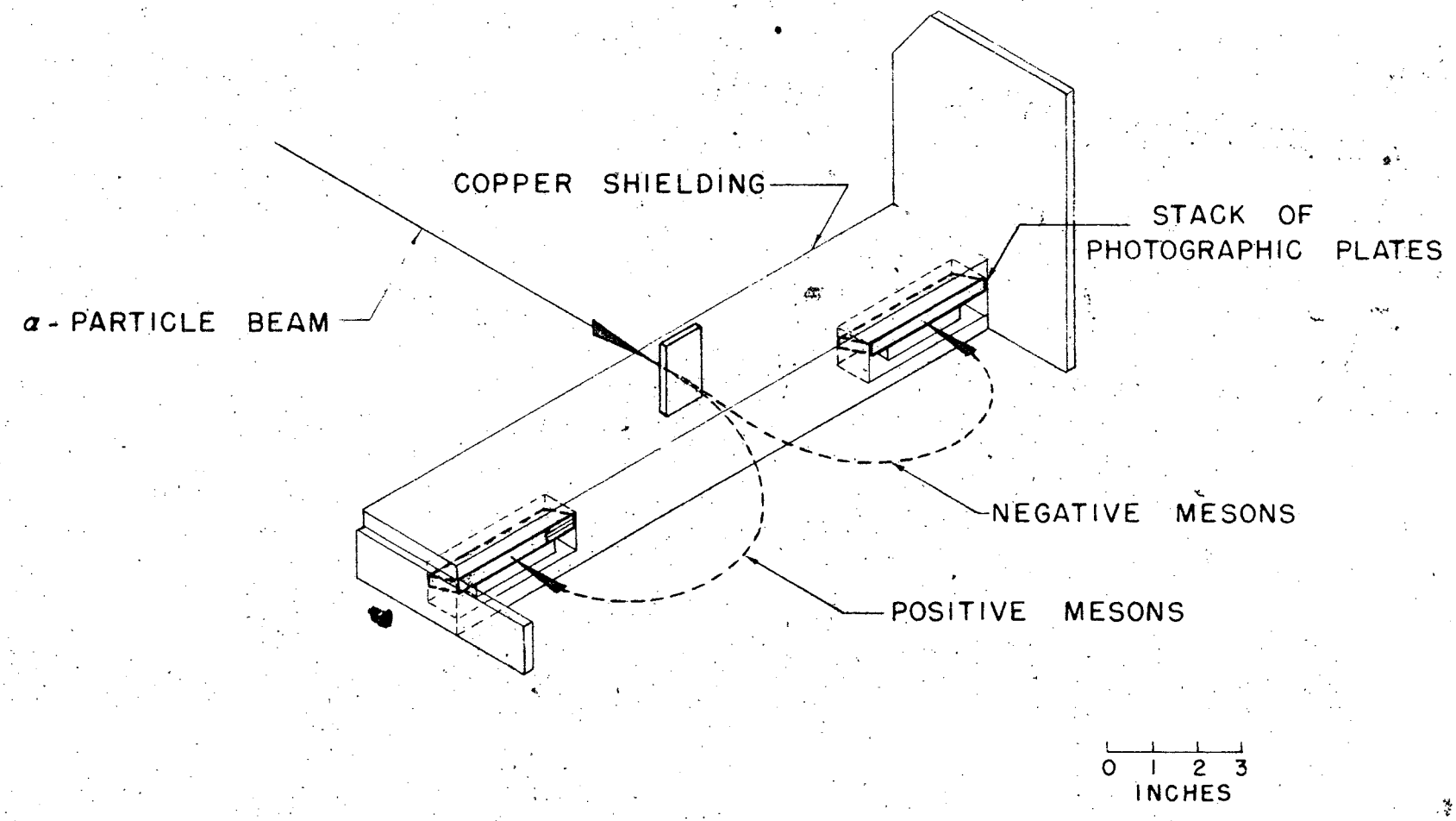
COPPER SHIELDING
STACK OF
PHOTOGRAPHIC PLATES
α - PARTICLE BEAM
NEGATIVE MESONS
POSITIVE MESONS
0 1 2 3
INCHES

FIG. 2

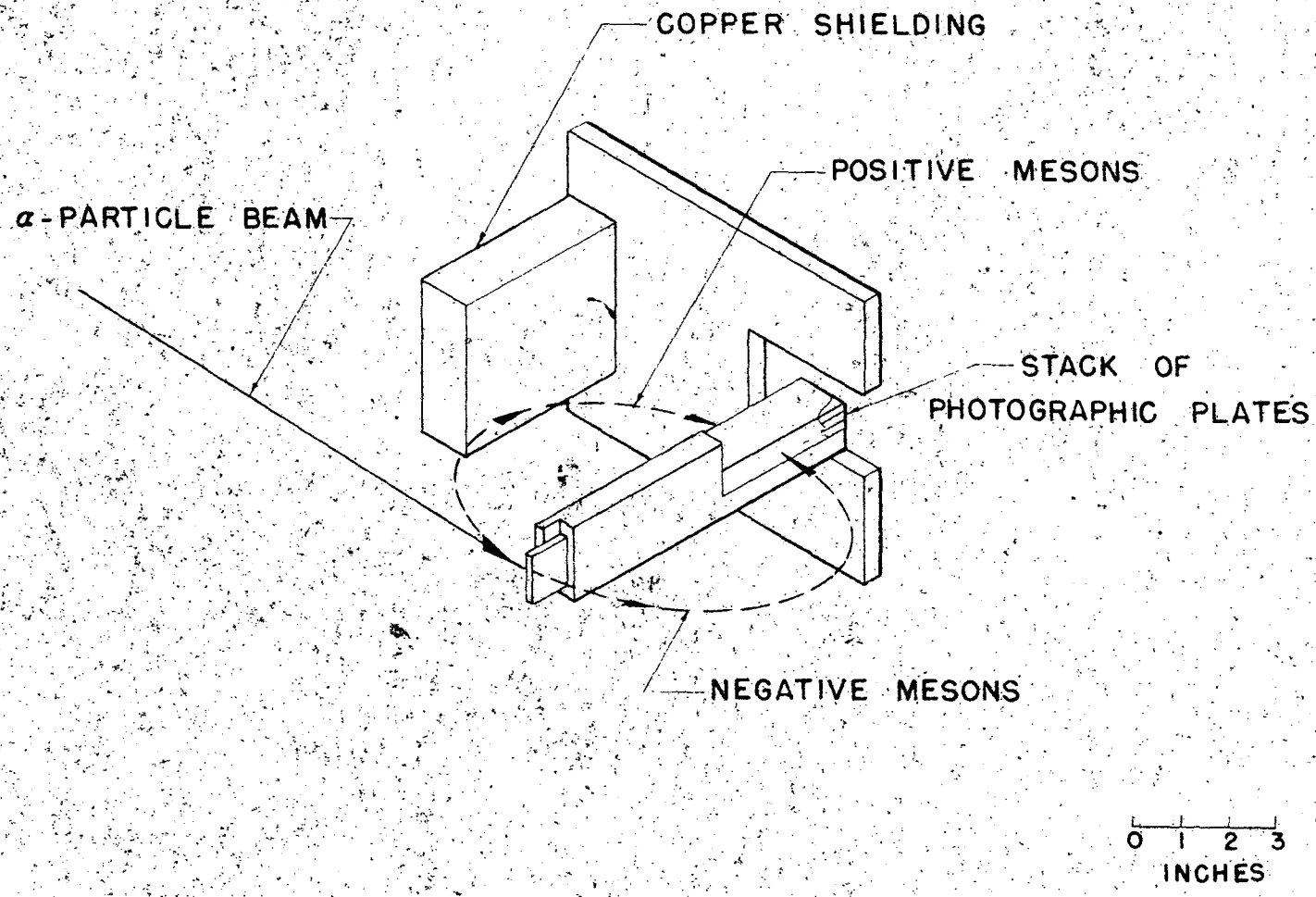
COPPER SHIELDING
POSITIVE MESONS
α-PARTICLE BEAM
STACK OF
PHOTOGRAPHIC PLATES
NEGATIVE MESONS
0 1 2 3
INCHES

FIG. 3

FIG. 4

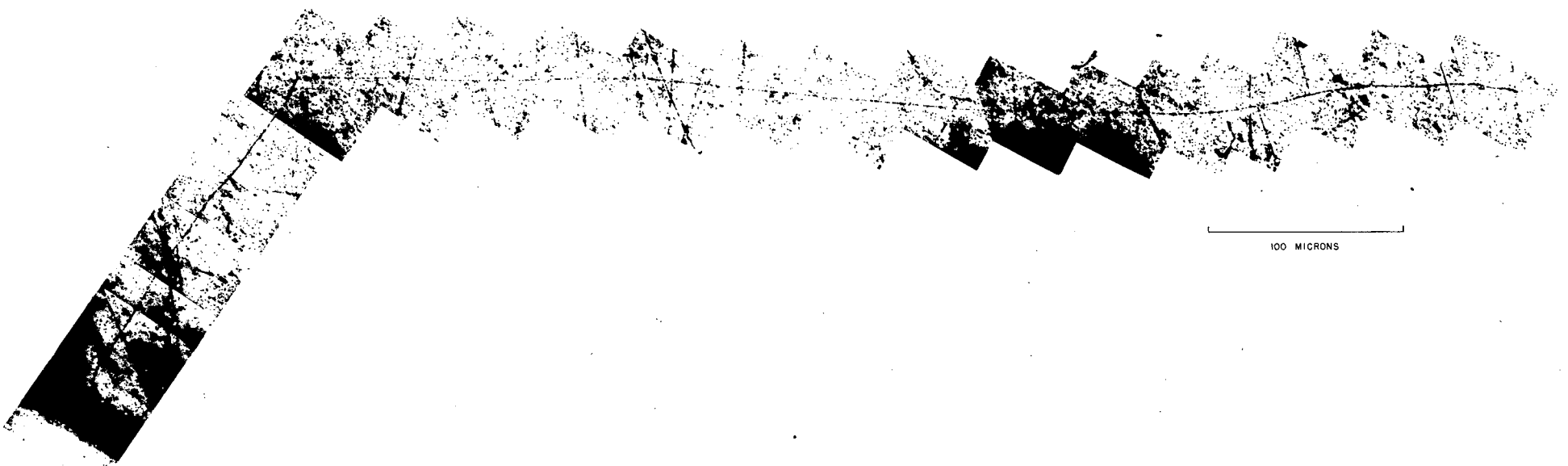

FIG. 5

3. Theoretical Physics

Robert Serber

Calculations have been made of the angular and energy distribution to be expected of the heavy mesons made by bombarding nuclei with α particles. In order to compare these predictions with experimental results, corrections must be made both for the selective effect of focussing in the magnetic field, and for the fact that the targets are not thin for the low energy mesons which are observed. The experimental results are too scanty to permit anything like a detailed comparison, but thin qualitative features seem to be satisfactorily explained. Using the theoretical energy and angular distributions, an estimate was made of the total cross section for production of mesons by 380 Mev alphas. This was found to be 10^{-29} cm^2 per carbon nucleus, or 2×10^{-31} cm^2 per nucleon-nucleon collision, in good agreement with the theoretical prediction by Horning. The difference in numbers of positive and negative mesons has been explained as an effect of the nuclear coulomb field. The magnitude of the effect is about right; more detailed calcualtions have not been completed.

Work is progressing on the influence of the shape of the potential on the predicted n-p scattering. Calcualtions have been made for Yukawa, exponential, gaussian and square wells. Perturbation calcualtions, which show the effect of a change of potential at a given radius have also been used to obtain more insight into the problem. We are now investigating whether a potential which is not so concentrated near zero radius as the more convential ones might give better results.

The shape of the straggling curves measured in the stopping power experiment with high energy deuterons can be fitted quite well to the theoretical curves. The comparison indicates that the deflected beam is homogeneous to about 1 Mev. Evidence has appeared that the mean ionization energy of non-metals differs from the linear law, $I = I_0 Z$, observed for metals.

Work is in progress on the elastic and inelastic cross sections of nuclei for high energy neutrons. Formulae for the cross sections in the case that nuclear matter has an index of refraction as well as an absorption coefficient for neutrons have been obtained. Comparison with the experimental results has not yet been completed.

A good deal of work has been done on synchrotron and cyclodrome problems.

4. Total Nuclear Cross Sections For High Energy Neutrons

N. Knable, J. DeJuren, B. J. Moyer

Total cross sections of twelve different elements for the neutron beam produced by bombarding a one-half inch beryllium target with 190 Mev deuterons in the 184-inch cyclotron have been measured with bismuth fission ionization chambers (1). The ionization chambers employed contained several discs in line coated with 1.5 mg/cm^2 of bismuth and were used both to monitor the intensity of the neutron flux and to detect the diminution of intensity caused by placing absorbers between a monitor chamber and a detecting chamber ten feet behind the monitor, all three in line with the axis of the collimated neutron beam.

The linear amplifiers used to detect the fission pulses were equipped with discriminators so as to limit the recording of pulses to those greater than the value of a bias voltage selected by the experimenter. The construction of the chambers was such that the discriminator voltage was proportional to the maximum energy of the fission pulses excluded from our records. Thus, in Fig. 1 we see a typical integral presentation of the disbribution of pulses in energy. The stability of the amplification and discriminating voltage was adequate to insure accuracy of the data to better than .5% as can be determined from both the stability of the amplifier voltages and the 1.5% volt variation of counting rate with discriminator potential. Discriminator curves were taken for several different neutron intensities in order to determine at what value of discriminator voltage the number of pulses due to multi-coincidences of spallation reactions became a measurable fraction of the number of fissions in bismuth.

The geometry of the experimental arragement was such that the solid angle subtended by the detector at the absorber was .0003 steradians. The effect of small angle scattering on the ratio of detector to monitor was investigated by halving the distance between absorber and detector using both absorbers of lead and of copper. The results of these experiments showed the change in the ratio caused by small angle scattering to be negligible for absorbers two mean free paths or less in length.

From the neutron spectrum and qualitative information on the variation of the bismuth fission cross section with energy, the mean energy of detection has been estimated to be 95 Mev.

The absorbers used in cross section measurements were all less than two mean free paths long. The effect of background was investigated by placing fourteen mean free paths of various absorbers between detector and monitor. The results are shown below.

Detector	Monitor	Absorber
950 fissions	1000 fissions	No absorber
0	3260	14 mean free paths of copper

The hydrogen cross section was measured by using 1.9 mean free paths of pentane and a carbon absorber of mass per unit area equal to the mass of carbon per unit area in the pentane, distributed over the same length. This technique obviates the necessity of a long counting interval without absorber to determine the cross sections of both pentane and carbon independently, as only counting intervals employing pentane and carbon are needed. We are thus able to replace a counting interval with no absorber, which in practice would not have an error of less than .4%, by a physical measurement of mass easily accurate to one part in 10,000. This measurement must be made with extreme accuracy in our case where the cross section desired is a small fraction of the carbon

cross section. The difference between the deuterium and hydrogen cross sections was determined in the same manner by using equal numbers of molecules per unit area of D_2O and H_2O.

The results are summarized in Table I below. The radii of the various nuclei are plotted in Fig. 2 as a function of the cube root of the mass numbers, where the radius is defined by

$$R = \sqrt{\frac{\sigma_T}{2\pi}}$$

Justification for using only two mean free paths of material to measure cross sections is obtained from the absorption curve of Fig. 3 which shows no deviation from an exponential decrease in neutron intensity with absorber thickness.

Table I

TOTAL CROSS SECTIONS FOR 90 MEV NEUTRONS MEASURED WITH BISMUTH FISSION CHAMBERS

Elements	Total Cross Sections $\sigma_T \times 10^{24}$ cm^2	Collision Radius R x 10^{13} cm
Hydrogen	.0745 ± .002 b.	
	.073 ± .003	1.08 ± .014
Deuterium	.105 ± .004	1.29 ± .03
Beryllium	.396 ± .004	2.51 ± .01
Carbon	.502 ± .004	
	.502 ± .005	
	.501 ± .006	2.83 ± .01
	.490 ± .004	
Nitrogen	.570 ± .007	3.01 ± .02
Oxygen	.663 ± .007	3.25 ± .02
Aluminum	.993 ± .011	3.98 ± .02
Chlorine	1.28 ± .02	4.51 ± .03
Copper	2.00 ± .02	5.64 ± .03
Tin	3.13 ± .025	7.06 ± .03
Lead	4.38 ± .03	8.35 ± .03
Uranium	4.89 ± .06	8.82 ± .05
Deuterium minus Hydrogen D-H	0.031 ± .002	
Compounds		
H_2O	.815 ± .005	
	.807 ± .005	
D_2O	.868 ± .005	
Pentane C_5H_{12}	3.40 ± .03	
	3.37 ± .03	
$C Cl_4$	5.61 ± .06	
Melamine $C_3H_6N_6$	5.37 ± .035	

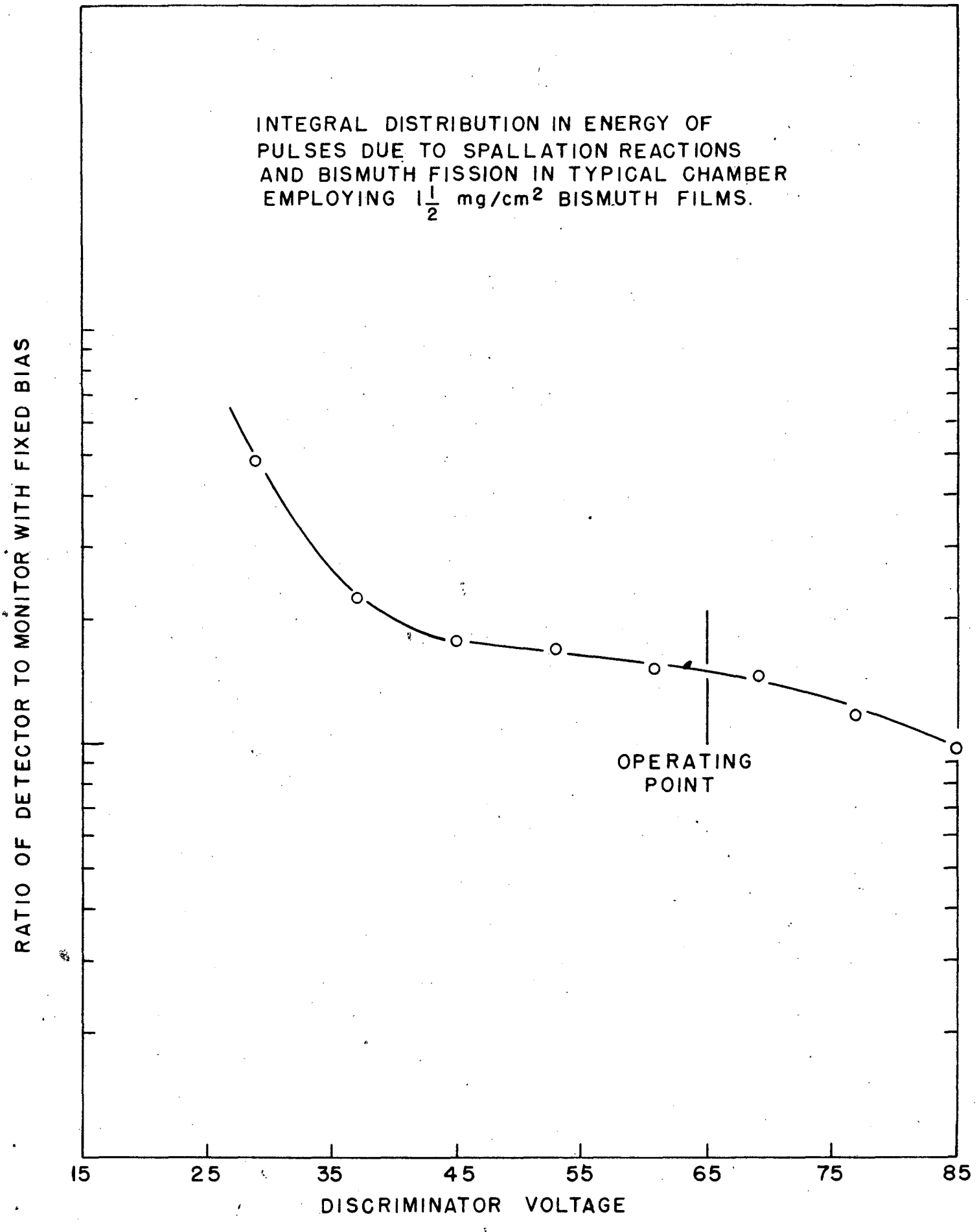
INTEGRAL DISTRIBUTION IN ENERGY OF PULSES DUE TO SPALLATION REACTIONS AND BISMUTH FISSION IN TYPICAL CHAMBER EMPLOYING 1 1/2 mg/cm2 BISMUTH FILMS.
RATIO OF DETECTOR TO MONITOR WITH FIXED BIAS
OPERATING POINT
15
25
35
45
55
65
75
85
DISCRIMINATOR VOLTAGE

FIG. 1

12688-1

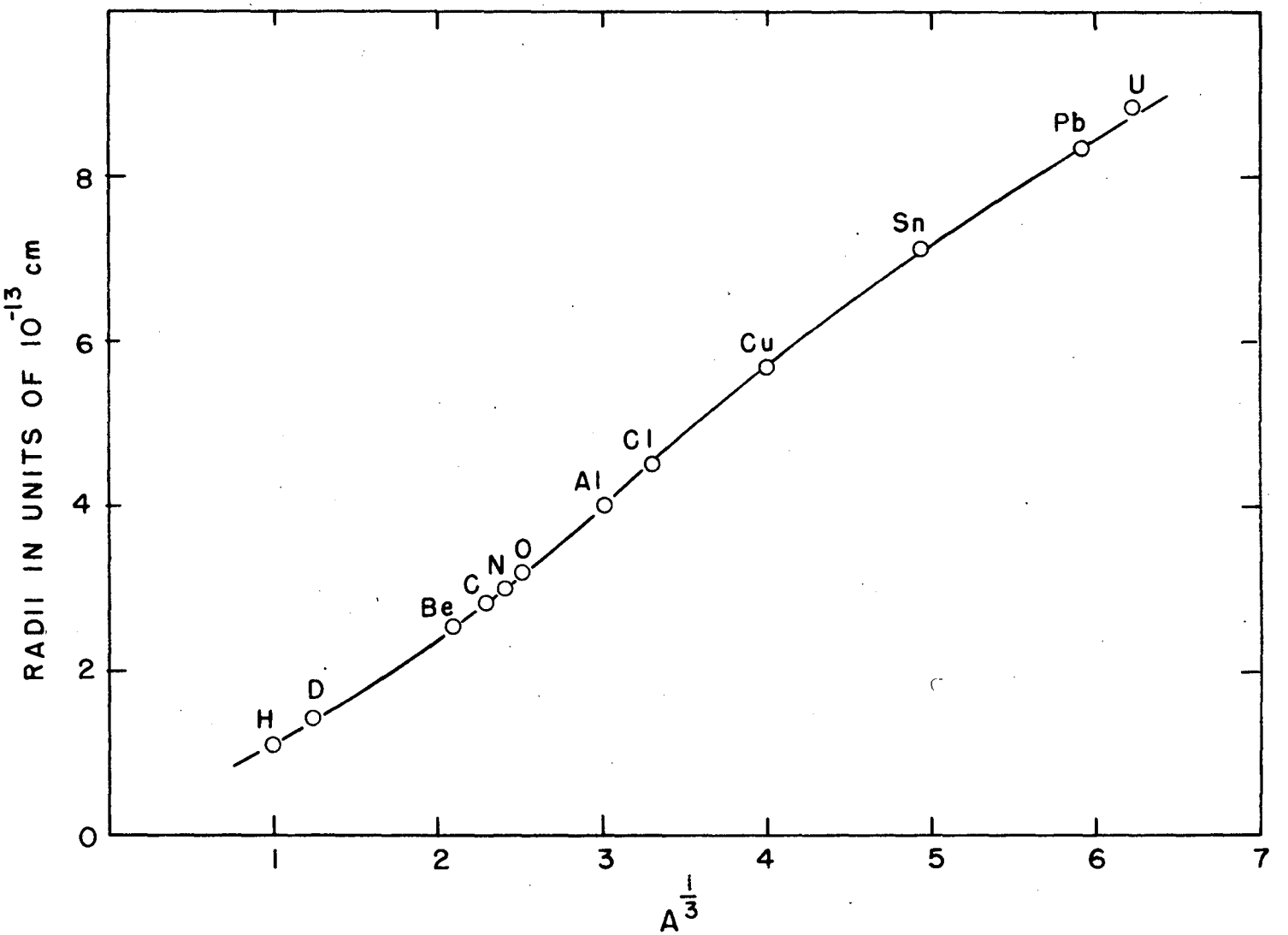
RADII IN UNITS OF 10^{-13} cm
0
2
4
6
8
1
2
3
4
5
6
7
$A^{\frac{1}{3}}$
H
D
Be
C
N
O
Al
Cl
Cu
Sn
Pb
U

FIG. 2

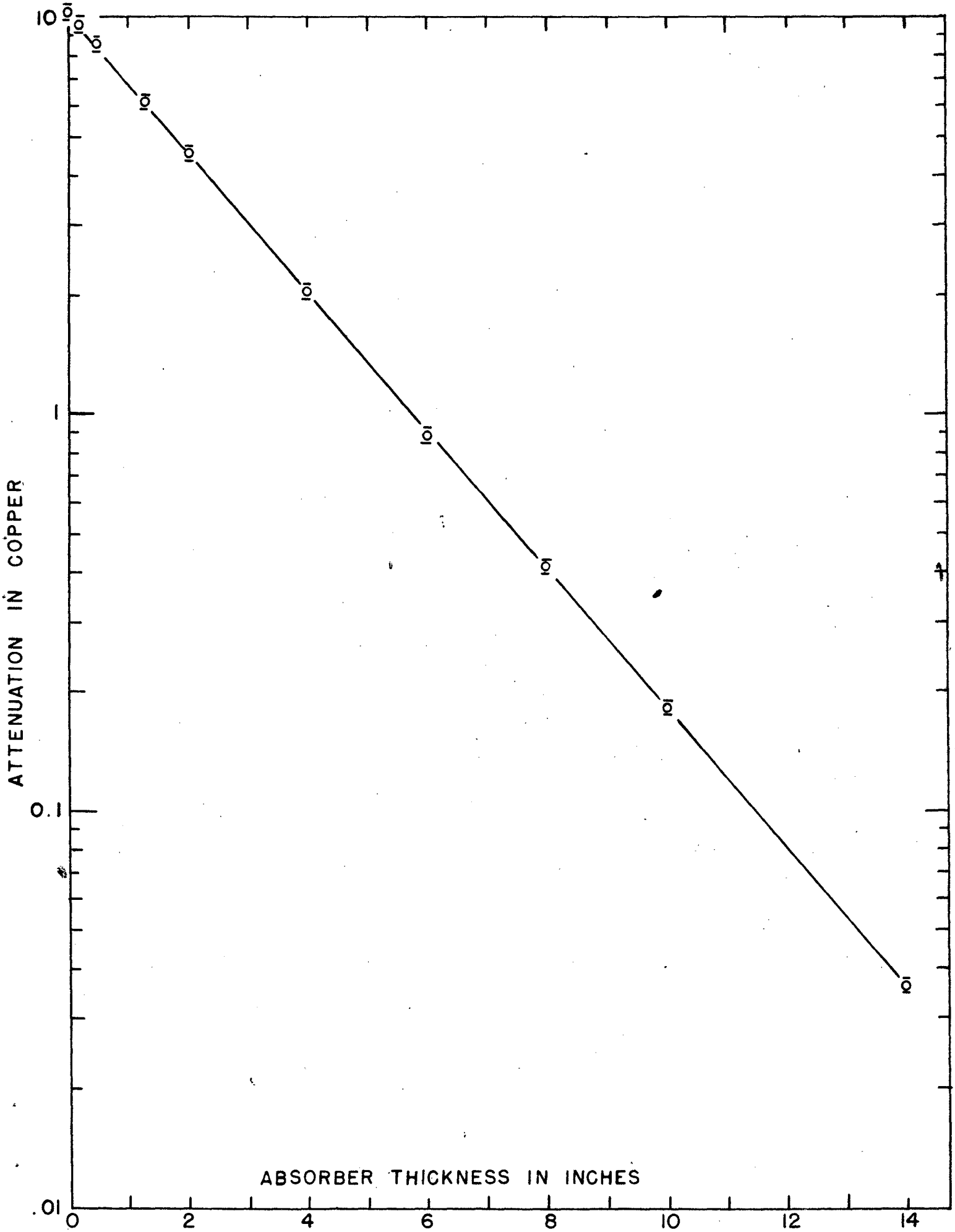
ATTENUATION IN COPPER
10
1
0.1
.01
ABSORBER THICKNESS IN INCHES
0
2
4
6
8
10
12
14

FIG. 3

5. Cross Section for the Reaction $C^{12}(n,2n)C^{11}$

Herbert F. York, Robert Mather

We have compared the cross section for producing C^{11} by the n,2n reaction on C^{12} with the differential n-p cross section at a fixed angle. This has been done at 40 Mev and 90 Mev and the results have been compared with a theoretical curve giving the relative cross section as a function of energy.

Experimental Arrangement

A small polyethylene disc weighing 250 mg/cm^2 was placed in the 90 Mev neutron beam and bombarded for twenty minutes. A proportional counter telescope with a 1" diaphram in front was placed facing the disc along a line making an angle of 25° with the neutron beam. The distance from the disc to the diaphram was 81 cm. All the protons from the disc which passed through the diaphram and had more than 48 Mev were counted for the entire bombardment. By making a second run with no scatterer, and using the usual methods of n-p scattering the number of protons produced by n-p collisions during the bombardment was determined.

After the bombardment, the polyethylene target was placed under a Geiger counter, and its beta activity was determined. The counter was calibrated by a standard uranium source. A 4 mg/cm^2 polyethylene disc was also bombarded in an intense neutron beam simultaneously with one of the 250 mg discs, in order to determine the correction for beta absorption in the thicker disc. It was necessary to use a thick disc in the runs made with the proportional counters because of the low intensity of the neutron beam outside the concrete shielding.

This procedure was repeated three times at 90 Mev then twice at 40 Mev, using an angle of 30° and appropriate absorber.

Calculation of the $C^{12}(n,2n)C^{11}$ Cross Section

The number (N_p) of protons per steradian per second from the CH_2 target at 25° above a certain energy E_{min} is given by

$$N_p = n_H \int_{E_{min}}^{\infty} N(E)\, \sigma_{np}(\phi, E)\, dE \qquad (1)$$

where

n_H = Number of H atoms in the CH_2 disc.
$N(E)$ = Neutron flux in a beam of energy E.
$\sigma_{np}(\phi,E)$ = Differential cross-section in the laboratory system for the scattering of protons into the angle ϕ at energy E.

Since in the n-p scattering experiment an average $\sigma_{np}(\phi)$ over the same distribution of neutron energies as used in this experiment has been measured, we may replace the $\sigma_{np}(\phi,E)$ above by $\overline{\sigma_{np}}(\phi)$ and remove it from the integral. Hence

$$N_p = n_H \overline{\sigma_{np}}(\phi) \int_{E_{min}}^{\infty} N(E)\, dE \qquad (2)$$

Similarly, the production of C^{11} per second (N_c) is given by

$$N_c = n_c \int_0^\infty \sigma_{C11}(E) N(E) dE \qquad (3)$$

In this experiment, because of the spread in energy of the neutron beam used, it is possible to calculate σ_{C11} only if some assumption about the shape of $\sigma_{C11}(E)$ is made. Two such shapes have been used; namely, the theoretical curve, and the curve σ_{C11} = constant over the energy distribution of the neutrons at each of the two energies used.

If we assume the shape of the theoretical curve to be correct, then

$$\sigma(E) = K f(E) \quad \text{and} \quad N_c = K n_c \int_0^\infty f(E) N(E) dE, \qquad (4)$$

where n_C = number of C atoms in the disc, and $f(E)$ = relative value of $\sigma_{C11}(E)$ as given by curve in Fig. 1. Thus

$$\frac{N_c}{N_p} = \frac{K}{2\overline{\sigma_{np}}(\phi)} \frac{\int_0^\infty f(E)N(E)dE}{\int_{E_{min}^{11}}^\infty N(E)dE} \qquad (5)$$

or

$$K = 2\overline{\sigma_{np}}(\phi) \frac{N_c}{N_p} \frac{\int_{E_{min}}^\infty N(E)dE}{\int_0^\infty f(E)N(E)dE} \quad ; \qquad (6)$$

If we assume σ_{C11} to be constant over the neutron energy distribution used, then

$$\overline{\sigma_{C11}}(E) = 2\overline{\sigma_{np}}(\phi) \frac{N_c}{N_p} \quad .$$

N(E) for the 90 Mev has been measured and is shown in Fig. 1. N(E) for 40 Mev is the theoretical curve calculated from the stripping process and is also shown in Fig. 1. Any low energy tail on N(E) at the lower energies would not affect the experiment, since these neutrons would produce neither countable protons nor C^{11}.

One check on the theory is to find whether K is the same (or nearly so) at 40 Mev and 90 Mev.

N_p is given by $$N_p = \frac{c}{\Omega t_b}\left(N_{CH_2} - N_B \frac{Mon_{CH_2}}{Mon_B}\right) \qquad (7)$$

where N_{CH_2} = Number of proton counts from a CH_2 disc.

N_B = Number of proton counts with no disc.

Mon_{CH_2} = Number of monitor counts during the bombardment of CH_2.

Mon_B = Number of monitor counts during blank run.

Ω = Solid angle subtended by proton diaphram.

t_b = Duration of the bombardment.

c = constant, determined from n-p experiments giving the fraction of CH_2 protons due to H; c = 0.76 for 25° and 90 Mev, c = 0.92 for 30° and 40 Mev.

$$N_C = g \frac{N_g - N_b}{(1 - e^{-\lambda t_b})e^{-\lambda t_i}(1 - e^{-\lambda t_g})} \qquad (8)$$

where g is the factor correcting for the geometry of the counter, as determined by comparison with a standard. g = 166 for the set up used. In this relationship

N_g = Number beta counts during the total beta counting time t_g.
t_b = Bombardment time
t_i = Time between the end of the bombardment and the beginning of the count.
N_b = Background counts for time t_g.

In the experiment, t_g was about 1200 seconds. N_g was twice background in the case of the 90 Mev bombardments, and three to four times background for the 40 Mev bombardment.

A typical set of data are

$\phi = 30^\circ$
Average E of neutrons = 40 Mev
E_{min} = 28 Mev
$C\left(N_{CH_2} - N_B \frac{Mon_{CH_2}}{Mon_B}\right) = 1480$
$\Omega = .763 \times 10^{-3}$
t_b = 1200 sec
N_g = 1600
N_b = 525
t_i = 300 sec
t_g = 1524 sec

The ratio of the integrals in equation (6) has been calculated numerically and is 5.22 for the 90 Mev bombardment and 4.16 for the 40 Mev bombardment.

The values of $\frac{N_c}{N_p}$ for the five runs made are

Run	$\frac{N_c}{N_p}$(90 Mev)	$\frac{N_c}{N_p}$(40 Mev)
I	0.480	
II	0.405	
III		0.238
IV		0.239
V	0.480	
Average	0.455	0.238

With these values and

$\overline{\sigma_{np}}$ (25°, 90 Mev) = 25.9 millibarns*

$\overline{\sigma_{np}}$ (30°, 40 Mev) = 48 millibarns*

*These values are at present only tentative

we get

K_{40} Mev = 96
K_{90} Mev = 123

While these two values of K are not identical, they are nearly so, compared to the ratio between the cross-section at 42 Mev and 90 Mev from the theoretical curve, namely 2.7. Using the values of K, and the theoretical f(E) we get

σ_{C11} (42) 37 millibarns
σ_{C11} (90) 17 millibarns

Assuming f(E) to be a constant over each neutron distribution, we get

$\overline{\sigma_{C11}}$ (40) 23 millibarns

$\overline{\sigma_{C11}}$ (90) 18 millibarns

However, since the neutron energy distribution at 40 Mev extends approximately from 27 to 51 Mev, and $\sigma_{C11}(E)$ must be quite small in the lower part of this range and then decrease again at higher energies, the existence of some sort of peak in the region around 40 Mev is quite probable.

Errors

The mean deviation from counting errors in determining the ratio $\frac{N_c}{N_p}$ is 6% at each energy. The errors in the absolute differential n-p cross sections are about 20%, though probably somewhat smaller relative to each other since each was determined in the same way. The $\sigma_{C11}(E)$ is flat in the high energy region theoretically, and hence the final error in σ_{C11}(90 Mev) is about 20%.

Figure 1

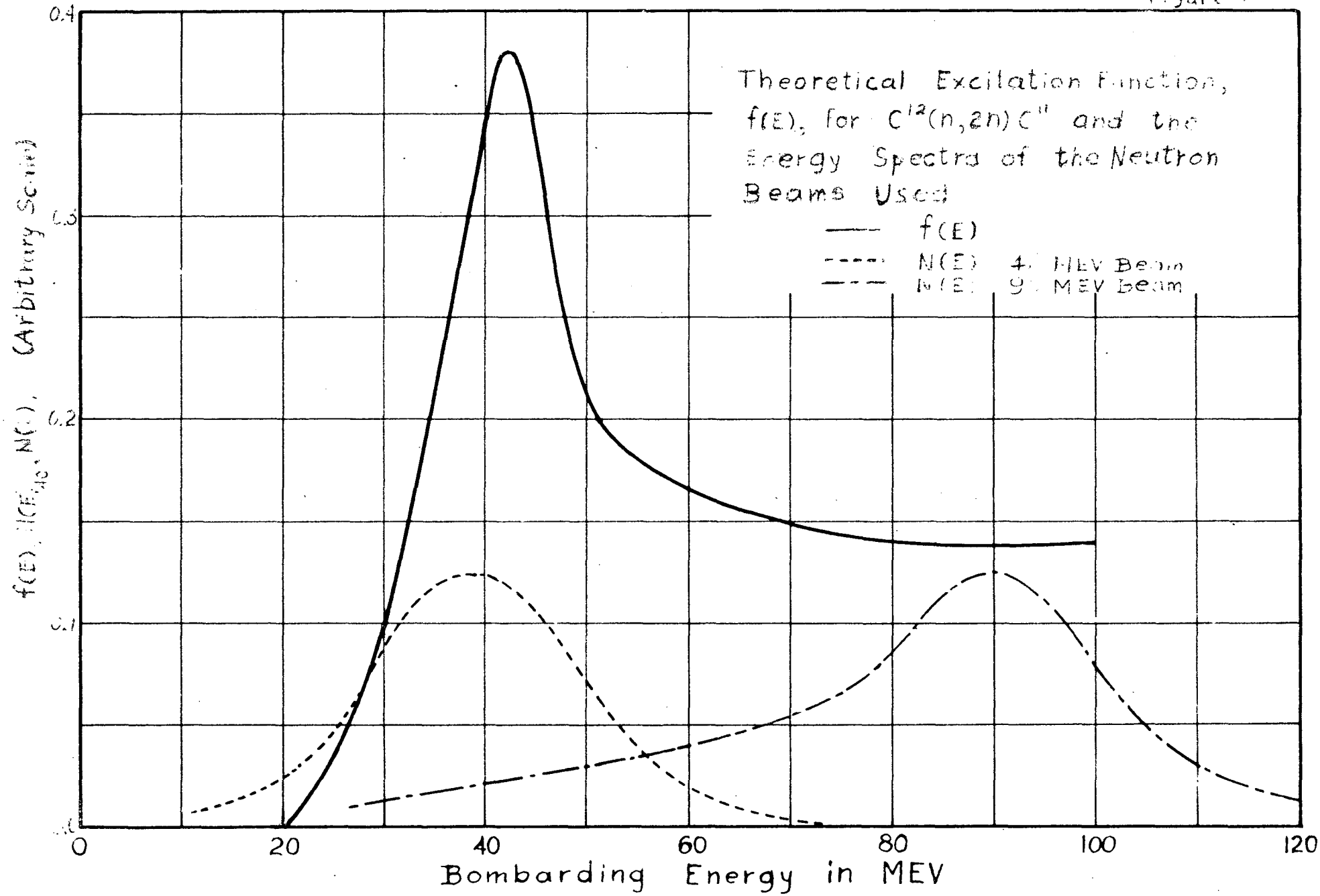

12713-1

6. 90 Mev Neutron Absorption and Scattering Cross Section

A. Bratenahl, R. Hildebrand, C. Leith, B. J. Moyer

The measurement of the angular distribution of elastically scattered neutrons from Al, Cu and Pb using the $C^{12}(n,2n)C^{11}$ reaction as a detector had previously indicated that the scattering cross section was greater than half the total cross section.

To check this result the angular distribution was redetermined using a coincidence telescope of proportional counters detecting the recoil protons out of paraffin. The essential change in this mode of detection consisted in raising the threshold of the detector from 20 Mev for carbon to 60 Mev for the coincidence counter. The results of the measurements with the two types of detectors agree within probable error. Angular distribution curves from these studies have been presented in a previous report. The approximate congruence of the curves obtained with the two detector thresholds suggests that inelastic events yielding scattered neutrons over 20 Mev must be relatively very infrequent.

To investigate further the relative contributions of elastic and inelastic processes to the total cross sections, an attenuation experiment was carried out using carbon detectors to determine simultaneously the good and poor geometry cross sections. The experimental arrangement is shown schematically in Fig. 1. The ratio $\frac{D_1}{M}$ determined approximately the absorption cross section; $\frac{D_2}{M}$ the total cross section; $\frac{D_2}{D_1}$ the elastic scattering cross section. Actually, the cone angle θ_0 was chosen to include all of the central peak of the elastic scattering distribution but omits part of the contribution of the wings of the distribution at large angles. Thus the poor geometry attenuation lacks the contribution of elastic scattering which is just the amount of scattering through angles greater than θ_0. The purpose of this limited geometry tends to allow a comparison to be made between the elastic scattering cross section obtained from this experiment and the cross section obtained from integration of the differential scattering cross sections out to θ_0 which was the practical limit of observation in the angular distribution experiments. The effect of the limited geometry is that it yields only an upper limit to the absorption cross sections and a lower limit to the scattering cross section, but the good agreement found between the two independent experiments indicate these limits are close to the true values.

An estimate of the correction due to the limited geometry was made by measuring the differential cross section out to very large angles with the proton recoil coincidence counter arrangement. An additional correction was made on the basis of an estimate of the contribution of detectable secondary particles registered by the detectors in the differential cross section measurements. Experimental data for this estimate came from studies of high energy protons emerging from elements bombarded in the neutron beam. The results of the attenuation experiments are as follows; the second figure in each column represents the cross section corrected for limited geometry and secondary production processes.

Element	Absorption Uncorrected	Absorption Corrected	Scattering Uncorrected	Scattering Corrected	Total
Al	0.46 ± 0.03	.40 ± .03	0.66 ± 0.03	.72 ± .03	1.12 ± 0.02
Ratio to total		.36		.64	
Cu	0.87 ± 0.02	.77 ± .06	1.25 ± .06	1.35 ± .06	2.12 ± .04
Ratio to total		.36		.64	
Pb	1.71 ± 0.11	1.59 ± 0.11	2.82 ± 0.13	2.94 ± 0.13	4.53 ± 0.09
Ratio to total		.35		.65	

These experiments indicate that the elastic scattering cross section is indeed larger than the absorption cross section; and the scattering cross sections here given are in reasonable agreement with those obtained by integrating the differential scattering cross sections previously measured.

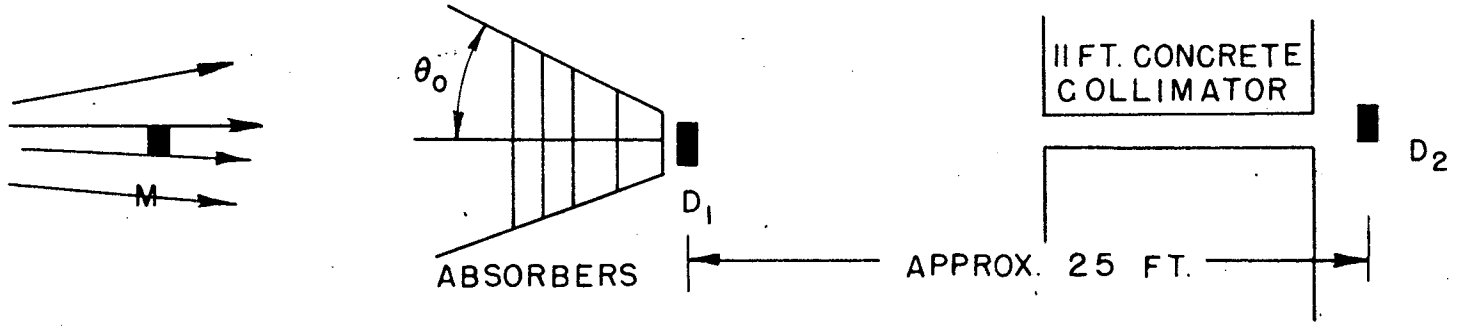
M
θ_0
ABSORBERS
D_1
11 FT. CONCRETE
COLLIMATOR
D_2
APPROX. 25 FT.

FIG. 1

7. Deuteron Range Measurements

Introduction

Range and relative stopping power measurements of the full energy deflected[1] beam of deuterons from the 184-inch Berkeley cyclotron have been made in conjunction with range-energy calculations made by Smith[2] of Cornell and by W. Aron, B. Hoffman, and others of Dr. Serber's Theoretical Group here.

The experimental method is essentially the same as that used by Wilson[3] (see Fig. 1) and consists of measuring the relative ionization of the deuterons for given thicknesses of absorber, then plotting the Bragg curve. The range of the deuterons was measured in aluminum, and the stopping power of elements relative to aluminum was measured for several elements ranging in Z from Be, Z = 4, to U, Z = 92.

Theoretical Considerations

It suffices to present here merely the $\frac{dE}{dx}$ equation[4] and a brief description of the method used by Aron, et al. in obtaining theoretical values for the range-energy relationship. The method is treated in detail in unpublished work of the Theoretical Group.

Assuming that the energy loss of charged particles passing through matter is due to the ionization and excitation of the atoms of the substance traversed, and further that the particle energy is much greater than the orbital electron velocities in the stopping material, the energy loss per unit distance per charged particle is

$$-\frac{dE}{dx} = \frac{4\pi N Z_1 \; Z_2^2 \; e^4}{mv^2} \left[\ln \frac{2\,mv^2}{(1-\beta^2)I} - \beta^2 \right] \qquad (1)$$

where; m is the electron mass, v the velocity of the charged particle of atomic number Z_2, Z_1 is the atomic number of the stopping material containing N atoms per cm^3, I is the average excitation energy of the atoms of the stopping material; e and β have their usual significance.

The theoretical range-energy curves were obtained by numerical integration of (1) with constants of integration being determined from the low energy ($\sim$8 Mev) experimental results of Wilson[3] and Mano[5].

Apparatus Description and Experimental Technique

Referring to Fig. 1, which shows the apparatus schematically, the detector ionization chamber is a thin (.5 inch) air filled chamber with a .0005" aluminum foil front wall and a 1-inch diameter collecting electrode. A monitor ionization chamber was placed in front of the absorber and this current read simultaneously with the detector chamber current, thereby eliminating the effect of beam fluctuations. The monitor chamber is a 1-inch thick air filled chamber with thin walls (.002") thus reducing the beam energy by a small amount. Monitor and detector chamber currents were measured by two R.C.A. Ultra-Sensitive D.C. meters, the detector to monitor ratio being plotted against absorber thickness to give the Bragg curve in Fig. 2.

Due to the dangerous level of radiation near the apparatus when the beam is on, the metering was done remotely and the absorber wheel was rotated remotely by means of a

selsyn system. Fig. 3 is a picture of the apparatus in position, ready for operation.

The relative stopping power measurements were done by working approximately at the midpoint of the steeply descending portion of the Bragg curve (see Fig. 2) and directly comparing relative ionization values of several aluminum thicknesses with a given thickness of the test element. In this manner a direct aluminum equivalent of each element tested was obtained.

Results

Since experiments are not yet completed, the results given here are preliminary and no attempts have been made to assign errors to the values given.

A typical experimentally obtained Bragg curve for deuterons in aluminum is shown in Fig. 2 From twenty separate determinations of the Bragg curve, the average mean range of the full energy deuterons from the 184-inch cyclotron in aluminum is 18.70 gms/cm^2. By assuming the range-energy values of Smith to be correct, it is possible to estimate the energy of the deuterons. The energy determined in this manner is ~194 Mev and is in good agreement with the $H\rho$ energy calculations made for the deflected beam. The root mean square of the straggling is ~1 Mev.

The stopping power data is treated in the manner used by Wilson, that is, the stopping power per electron of the various elements is compared with that of aluminum.

Defining
$$q = \frac{(\Delta R \cdot Z/A)_{Al}}{(\Delta R \cdot Z/A)_{X}}$$

where; ΔR_{Al} is the aluminum equivalent thickness of a thickness ΔR_X of element X; and plotting q vs log Z the very good approximation to a straight line shown in Fig. 4 is obtained. Work is being continued on some other elements, principally non-conductors, and on the elements shown to obtain better statistics.

References

1. Description of deflector system in UCRL-66, p. 41, by D. C. Sewell

2. Phys. Rev. 71, 32 (1947)

3. Phys. Rev. 60, 749 (1941)

4. Bethe, Rev. Mod. Phys. 9, 261 (1937)

5. Ann. de Phys. 1, 407 (1934)

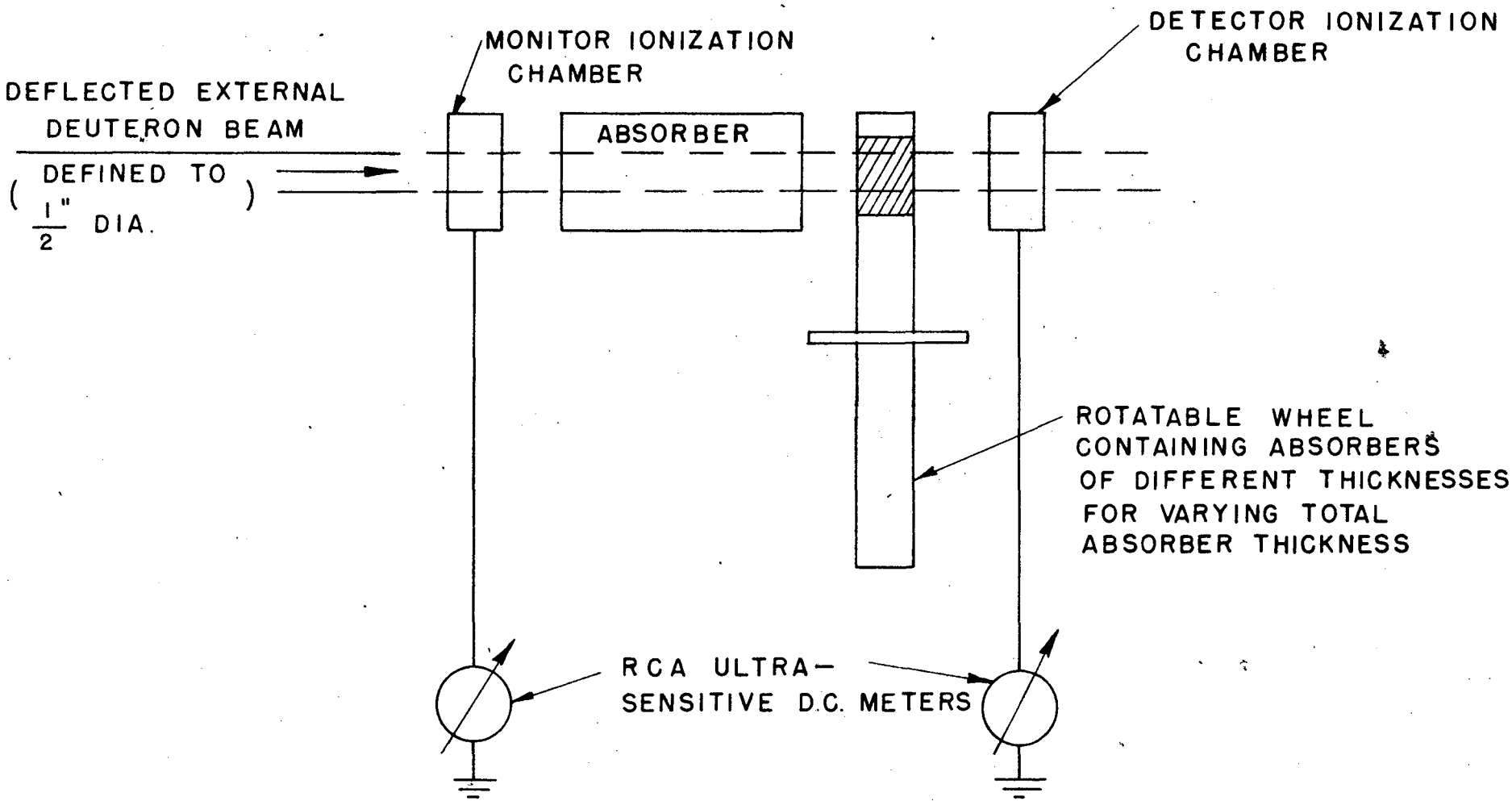
MONITOR IONIZATION CHAMBER
DETECTOR IONIZATION CHAMBER
DEFLECTED EXTERNAL DEUTERON BEAM
(DEFINED TO 1/2" DIA.)
ABSORBER
ROTATABLE WHEEL CONTAINING ABSORBERS OF DIFFERENT THICKNESSES FOR VARYING TOTAL ABSORBER THICKNESS
RCA ULTRA-SENSITIVE D.C. METERS

FIG. 1

12692-1

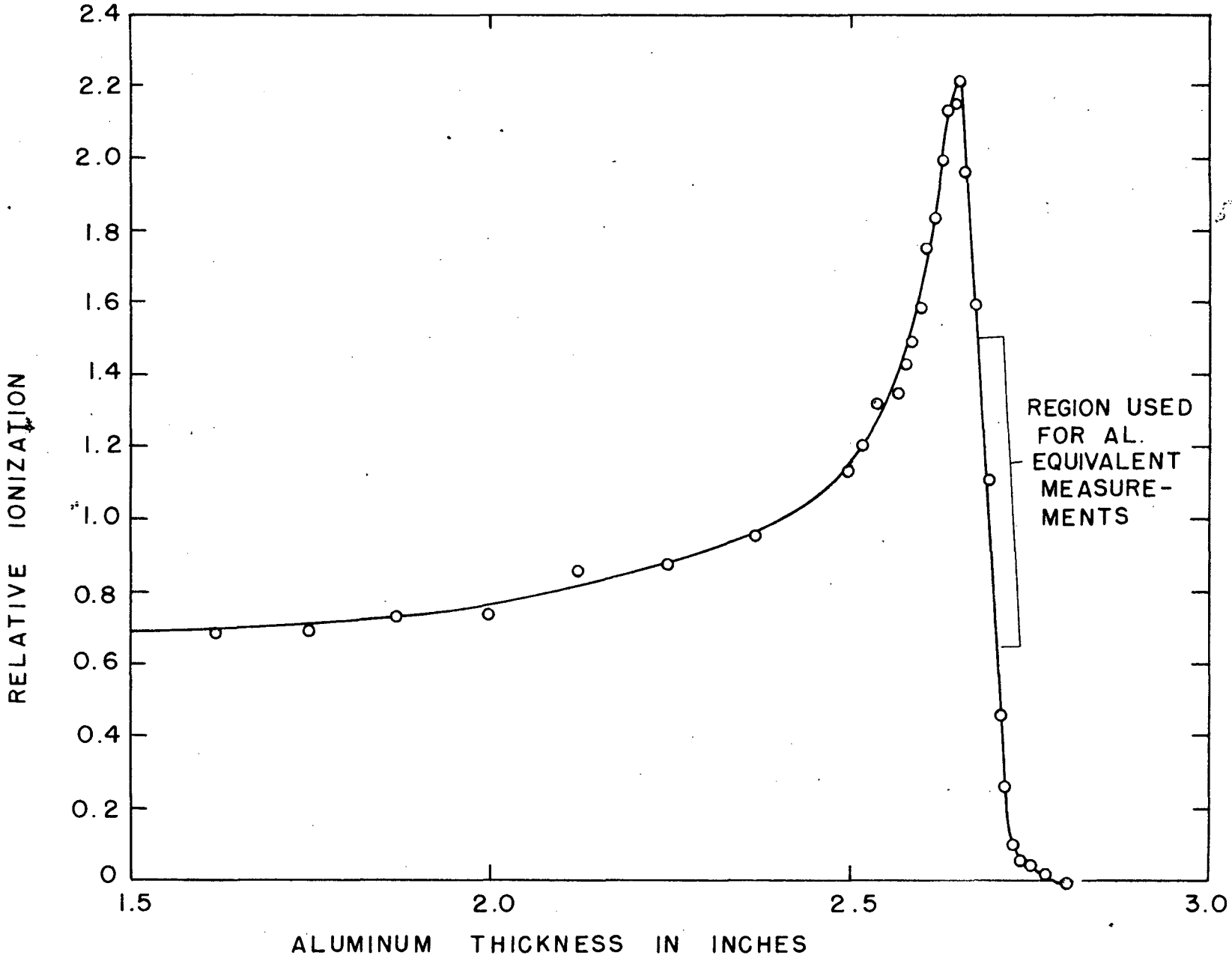

FIG. 2

BRAGG CURVE FOR FULL ENERGY DEFLECTED DEUTERONS IN ALUMINUM

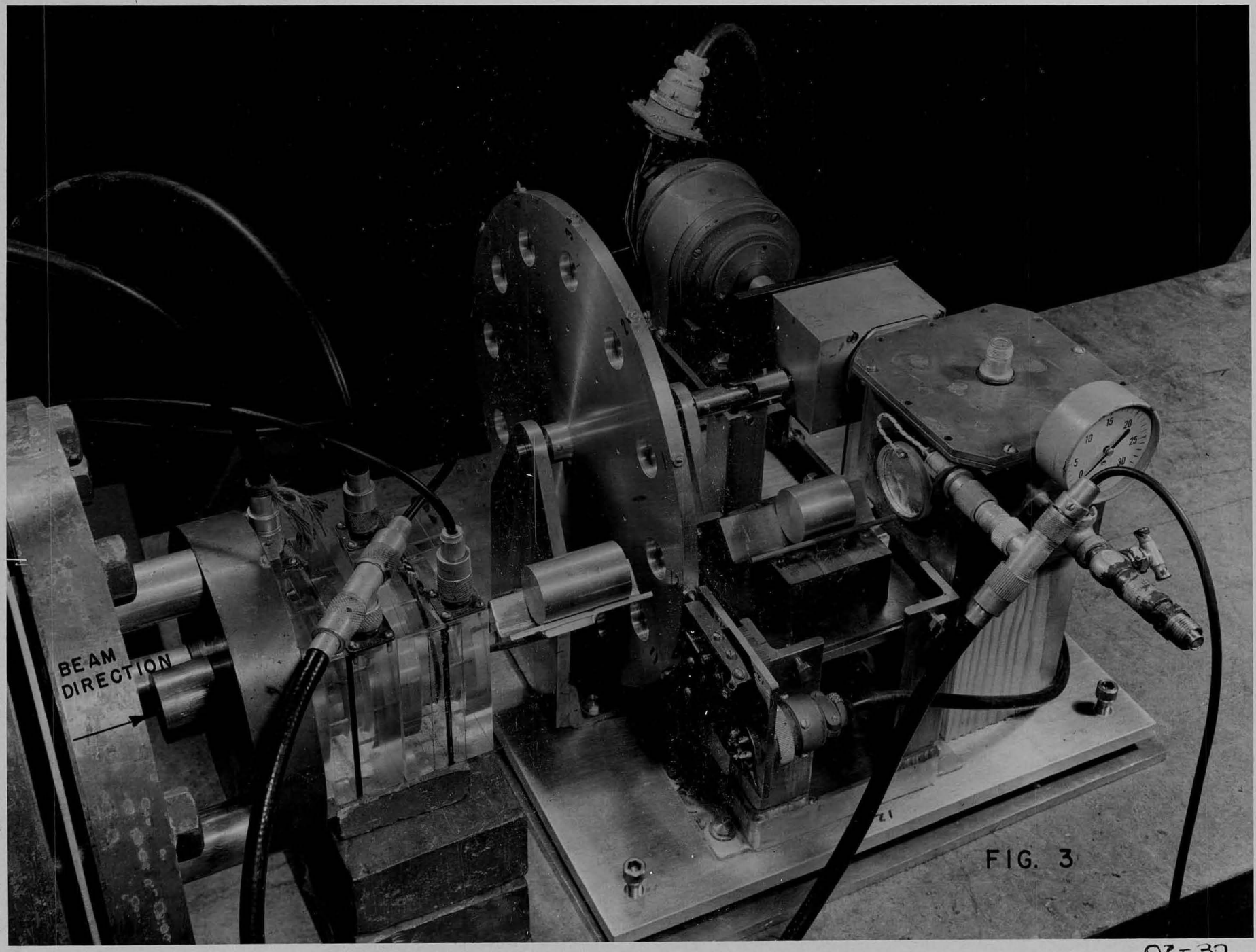

FIG. 3

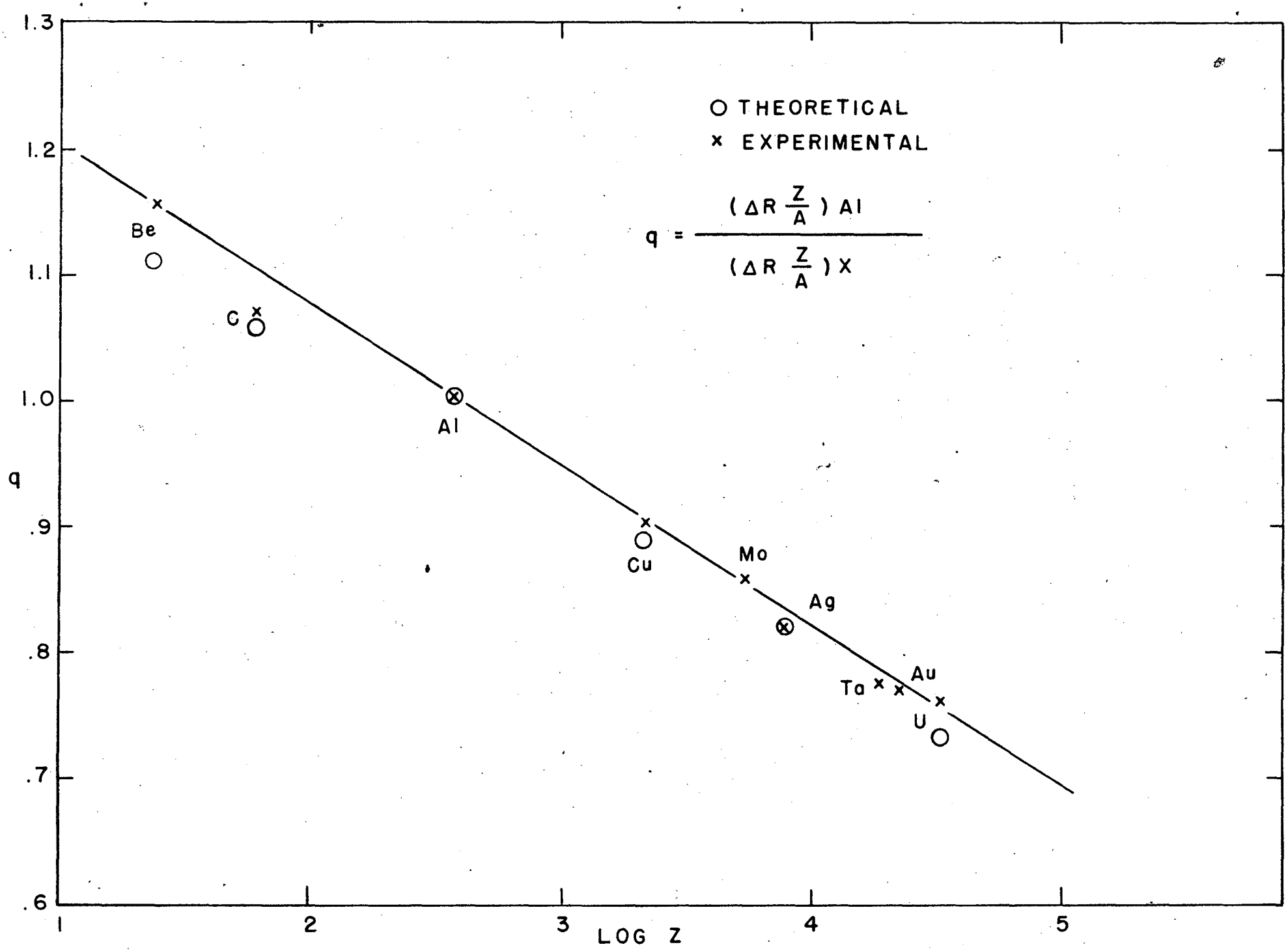

FIG. 4
FOR FULL ENERGY DEFLECTED DEUTERONS

12694-1

8. n-p Scattering and the Distribution of Fission Fragments from High Energy Neutron Fission

E. Segrè

In the last three months we have completed the experiments on n-p scattering at 45 and 90 Mev. A comprehensive paper on this subject has been prepared for publication, and since it is expected that it will be ready for declassification within a very short time, it will not be reported here.

The study of n-p scattering is part of the study of the interaction between elementary particles. We hope to complete it with a study of p-p scattering by techniques very similar to the ones used on n-p scattering as soon as a deflected proton beam becomes available.

The n-n scattering, necessary to complete the picture, cannot be studied directly, but a study of p-d and n-d scattering combined with n-p and p-p scattering data may probably be interpreted theoretically to deduce information on n-n scattering. Elastic scattering should be investigated first and inelastic scattering possibly later. Plans for experiments on this subject have been and are under study. At present it seems that the most promising line of attack for n-d scattering may be to scatter the neutron beam in deuterium in the cloud chamber; and for p-d scattering to bombard hydrogen with the deuteron beam and use counter techniques.

We have also started an investigation on the ionization produced by single fission fragments, when the fission is produced by 90 Mev neutrons. The curve relating the number of fragments with the ionization produced by the fragments has characteristically two peaks if fission is produced by low energy neutrons. With high energy neutrons the two peaks merge into one, in agreement with what is to be expected from the previous findings by the chemical investigation of the distribution of the masses of fission fragments. The maximum energy spent by a single fragment and the average energy of the fragments do not seem to differ materially in the cases of 90 Mev or low energy neutron fission. This fact is susceptible of various interpretations and only further experiments can tell which one is to be accepted.

9. The Half Lives of Aluminum^{25} and Aluminum^{26}

Hugh Bradner and J. D. Gow

The availability of separated isotopes of Mg makes it easy to determine the half life of Al^{25}, a member of the Wigner series which has long been suspected to have a half life of approximately 7 seconds, but which has not been confirmed because of the masking 7 second activity of Al^{26}.

Mg^{24}, Mg^{25} and Mg^{26} (in the form of MgO) have been bombarded with protons from the Berkeley Linear Accelerator, with the following results:

Mg^{24} yields an activity of approximately 23 seconds half life, presumably due to Na^{21} from the reaction $Mg^{24}(p,\alpha)Na^{21}$.

The Mg^{25} yields an activity of approximately 8 seconds half life, which we assign to the reaction $Mg^{25}(p,n)Al^{25}$.

The Mg^{26} yields an activity of approximately 6 seconds half life, assigned to Al^{26} according to a similar reaction.

It seems probable therefore that the 7 seconds half life normally given for Al^{26} is a mixture of these two activities.

10. Evidence For a p,d Reaction in Carbon

Wolfgang K. H. Panofsky and Robert Phillips

The reaction $C^{12}(p,pn)C^{11}$ has been investigated at proton energies up to 140 Mev in the 184-inch cyclotron by Chupp and McMillan[1] and McMillan and Miller[2], both as to excitation and absolute cross section. The high energy behavior of this reaction is taken as evidence for the ideas of Serber[3] explaining these processes by a direct knockout, rather than a compound nucleus process.

In this experiment excitation curves of this reaction were obtained in the region from threshold to 32 Mev using the Berkeley linear accelerator. Stacks of polystyrene (C_nH_n) foils were bombarded in the beam of the accelerator; specially molded 10 mil (25 mg/cm^2) foils were used from 32 Mev to 21 Mev, commercial 5 mil and 2.5 mil foils were used from 21 Mev to 16 Mev. All foils were weighed and calibrated for uniformity. The β^+ from C^{11} were counted in standard geometry in a thin window G.M. counter and compared with a UO_2 standard sample. The resultant curve is shown in Fig. 1. The absolute cross sections were obtained by bombarding a foil at 32 Mev in vacuo and collecting the protons in a Faraday cup. The beam passed through an open cylinder maintained at 8,000 volts in going from the sample to the collector cup. The current to the cup was integrated on a low leakage condenser and the voltage read on a balanced electrometer. The entire electrometer apparatus is in vacuo. Bombardments were also made with the sample located directly in the collector cup and gave results in agreement with the results obtained when bombarding in the beam ahead of the secondary electron suppressing cylinder. The result is

$$\sigma_{32\ \mathrm{Mev}} = (.075 \pm .02) \times 10^{-24}\ \mathrm{cm}^2$$

The probable error is entirely due to the problem of absolute evaluation of the β-ray standard. Further work on improving the precision of the absolute β^+ count is planned. The internal consistency is $\pm$ .0004 barns over 8 runs.

The energy scale in Fig. 1 was established by the use of a range-energy relation in polystyrene as computed by Mr. Henrich of this laboratory. To check the correctness of this relation, a run was made substituting Al Absorbers[4] to energies down to 20 Mev and using polystyrene absorbers below this point. The resultant points, shown by X in Fig. 1, are indistinguishable from the polystyrene absorber points. The range-energy relation was checked also by absorbing the 32 Mev beam down to the threshold of the $B^{11}(p,n)C^{11}$ reaction which was found to be 2.97 $\pm$ .1 Mev by Haxby, Shoupp, Stephens and Wells[5]. We obtain 3.0 $\pm$ .3 Mev indicating that the accuracy at the end point of the $C^{12} \rightarrow C^{11}$ reaction is of the order of $\pm$ .1 Mev. The output energy of the linear accelerator is inferred from frequency and drift tube dimensions to be 32.0 $\pm$ .1 Mev, an extrapolated range measurement in Al gave 32.1 $\pm$ .1 Mev.

If we assume that the threshold of the reaction is sharp, then the threshold can be located from the maximum of the second derivative curve. (Fig. 1) We place the threshold of the reaction at

$$18.5 \pm .3\ \mathrm{Mev}$$

If we take the mass of C^{11} to be 11.01498 (in agreement with the threshold[5] of 2.97 Mev for $B^{11}(p,n)C^{11}$, and the β^+ end-point[6] from C^{11} of .95 Mev) the calculated threshold of the reaction $C^{12}(p,pn)C^{11}$ corrected for recoil, is 20.2 Mev. The earlier values given by Livingston and Bethe and Barkas[7] for the C^{11} β^+ end-point and the mass of C^{11} are about .3 Mev higher but are based on earlier measurements[8] probably affected by N^{13} contamination. This means that the reaction $C^{12} \rightarrow C^{11}$ must be a (p,d) reaction, rather than

a (p,pn) reaction, at least near the excitation threshold. The only other instance of a specific deuteron yielding reaction known is the reaction $Be^9(p,d)Be^8$ (9). Cosmic ray evidence in photographic plates(10) makes it appear that such an event is also possible in high energy processes without breakup of the deuteron.

If the incoming proton were captured by the C nucleus, the resultant excited N^{13} would strongly favor energetically the re-emission of a proton over the emission of a deuteron or neutron. The cross section of the p,d reaction by a compound nucleus process should therefore be much smaller than the values observed. The process is therefore likely to take place by a direct interaction, e.g. by direct ejection of a deuteron and subsequent decay of proton unstable N^{12}.

References:

(1) Chupp and McMillan, Phys. Rev. 72, 873 (1947)
(2) McMillan and Miller, Phys. Rev. 73, 80 (1948)
(3) R. Serber, Phys. Rev. 72, 1114 (1947)
(4) J. H. Smith, Phys. Rev. 71, 32, (1947)
(5) Haxby, Shoupp, Stephens and Wells, Phys. Rev. 58, 1035 (1940)
(6) Delsasso, White, Barkas and Creutz, Phys. Rev. 58, 586 (1940)
Siegbahn, Arkiv. Mat. Astr. Fysik 30A, No. 20, (1944)
30B, No. 3, (1944)
(7) Livingston and Bethe, Rev. Mod. Phys. 9, 245 (1937)
Barkas, Phys. Rev. 55, 691 (1939)
(8) Fowler, Delsasso and Lauritsen, Phys. Rev. 49, 561 (1936)
(9) Allison, Skaggs and Smith, Phys. Rev. 54, 171, (1938)
J. S. Allen, Phys. Rev. 51, 182 (1937)
(10) LePrince-Ringuet, Cosmic Ray Conference, Pasadena, June, 1948

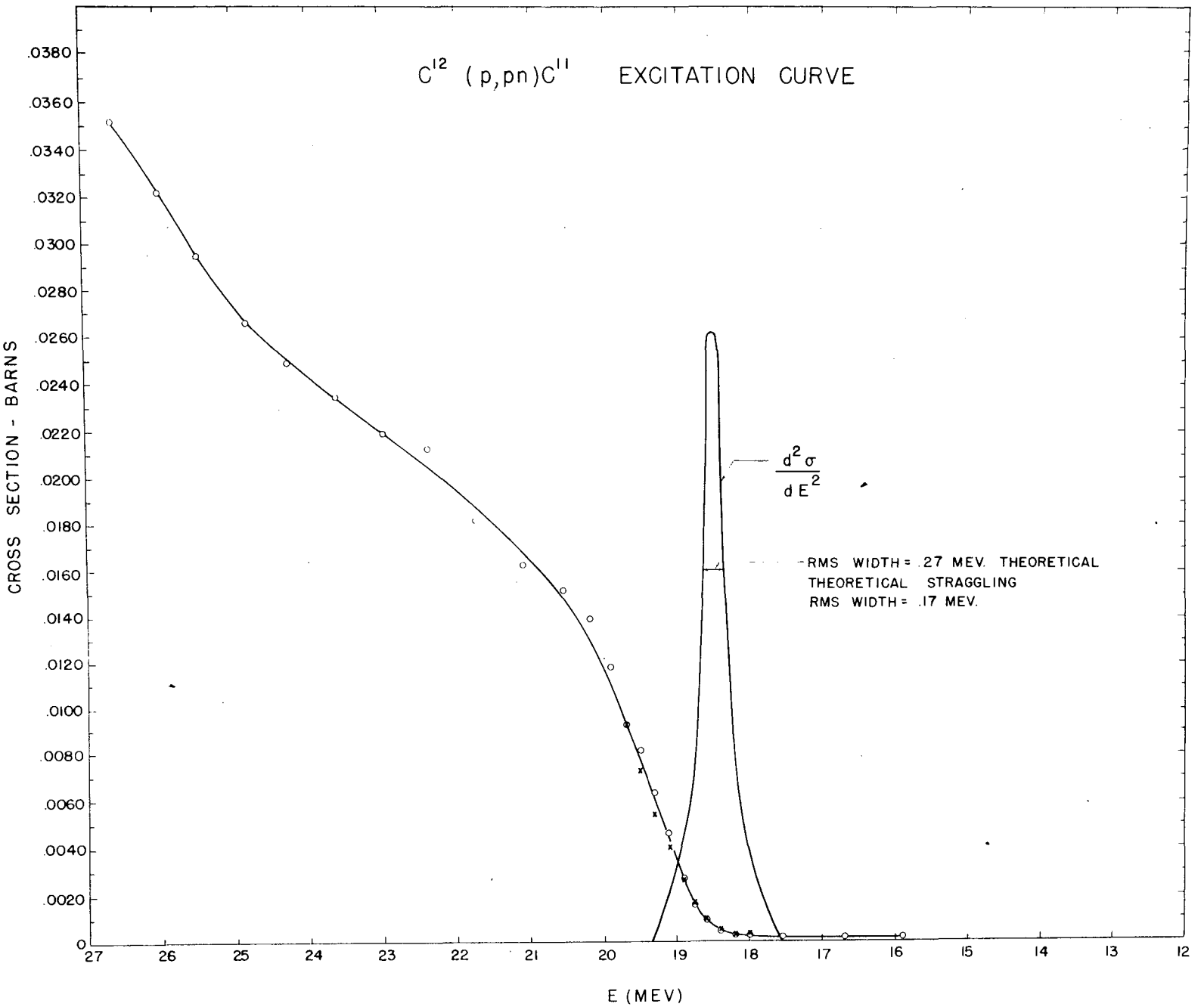
C^{12} (p,pn)C^{11} EXCITATION CURVE
CROSS SECTION - BARNS
.0380
.0360
.0340
.0320
.0300
.0280
.0260
.0240
.0220
.0200
.0180
.0160
.0140
.0120
.0100
.0080
.0060
.0040
.0020
0
27
26
25
24
23
22
21
20
19
18
17
16
15
14
13
12
E (MEV)
$\frac{d^2\sigma}{dE^2}$
RMS WIDTH = .27 MEV. THEORETICAL
THEORETICAL STRAGGLING
RMS WIDTH = .17 MEV.

FIG. 1

OZ-1

II. ACCELERATOR AND CALUTRON OPERATION AND DEVELOPMENT

1. 184-inch Cyclotron

James Vale

Proton Conversion

The proton conversion unit has been assembled and vacuum tested as far as possible before its installation in the cyclotron tank. At the completion of the vacuum tests, the new dee was installed (see Fig. 1) on the unit, and dummy pole pieces were built above and below the dee. This structure is necessary for the radio-frequency test which is now in progress.

The proton conversion rotary condenser has been designed to eliminate certain difficulties encountered with the present condenser. All water cooled insulators have been eliminated in the rotor (see Fig. 2).

The oscillator, as in the present system, is housed in a removable unit (see Fig. 3). It is planned to install the proton unit immediately upon completion of the radio-frequency tests.

Neutron Beam Backstop

During certain runs in the past, involving the neutron beam outside the concrete shielding, but inside the building, the neutron beam was allowed to emerge from the building. A barrier to this neutron beam has been constructed and consists of a block of concrete placed just inside the wall of the building. The beam level just outside the building at this point is now reduced to an extremely low value.

Neutron Beam Telescope

A second telescope has been constructed for further ease of aligning equipment in the neutron beam. This telescope fits on the neutron bench and is light enough so that it can be removed after use. This telescope can be used for alignment with the two neutron beams that are available.

Stairway to Top of Magnet

A permanent steel stairway has been built to provide access to the area on top of the 184-inch magnet. This stairway eliminates the hazards that were present with the ladders used previously.

Concrete Shielding

The concrete blocks for the permanent deuteron cave have been designed. The permanent cave will have a concrete roof and thus allow use of the overhead crane during those periods in which the deuteron beam is brought out of the tank. In addition, during these periods, the roof should reduce still further the general neutron background in the

building. The cave will have five feet of concrete in the walls with three feet thick roof blocks.

Flipper Probe

During the course of the meson experiments, it was found that a monitor other than a Zeus meter is necessary for the proper resolution of the alpha and deuteron beams. Therefore, a monitor was constructed which takes advantage of the fact that at any one radius the alpha beam has one-half the range in a given material of the deuteron beam. This probe allows two currents to be read simultaneously and operating conditions can thus be adjusted to discriminate one beam against the other. Furthermore, this monitor has been installed permanently inside the vacuum tank and can be inserted into the beam by means of a coil mounted on it.

Target Mounting on Probe Heads

A fast acting holder for targets on probe heads has been developed to minimize handling time of radioactive targets after bombardment in the cyclotron. These targets are held on the probe by spring action rather than screws and can be simply slipped off the probe with a long handle. This will reduce exposure to radiation during the transfer of such targets.

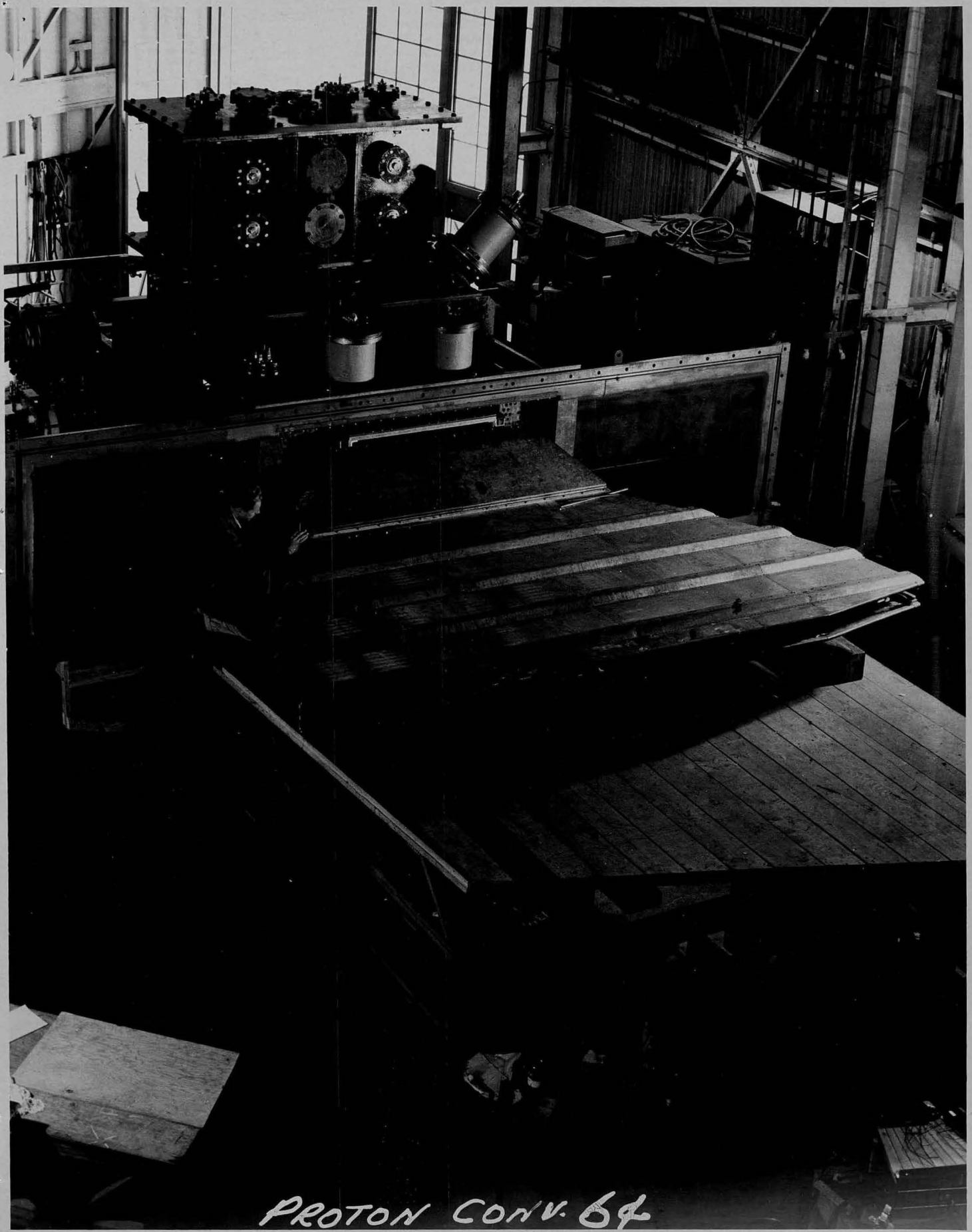

PROTON CONV. 64

OZ-121

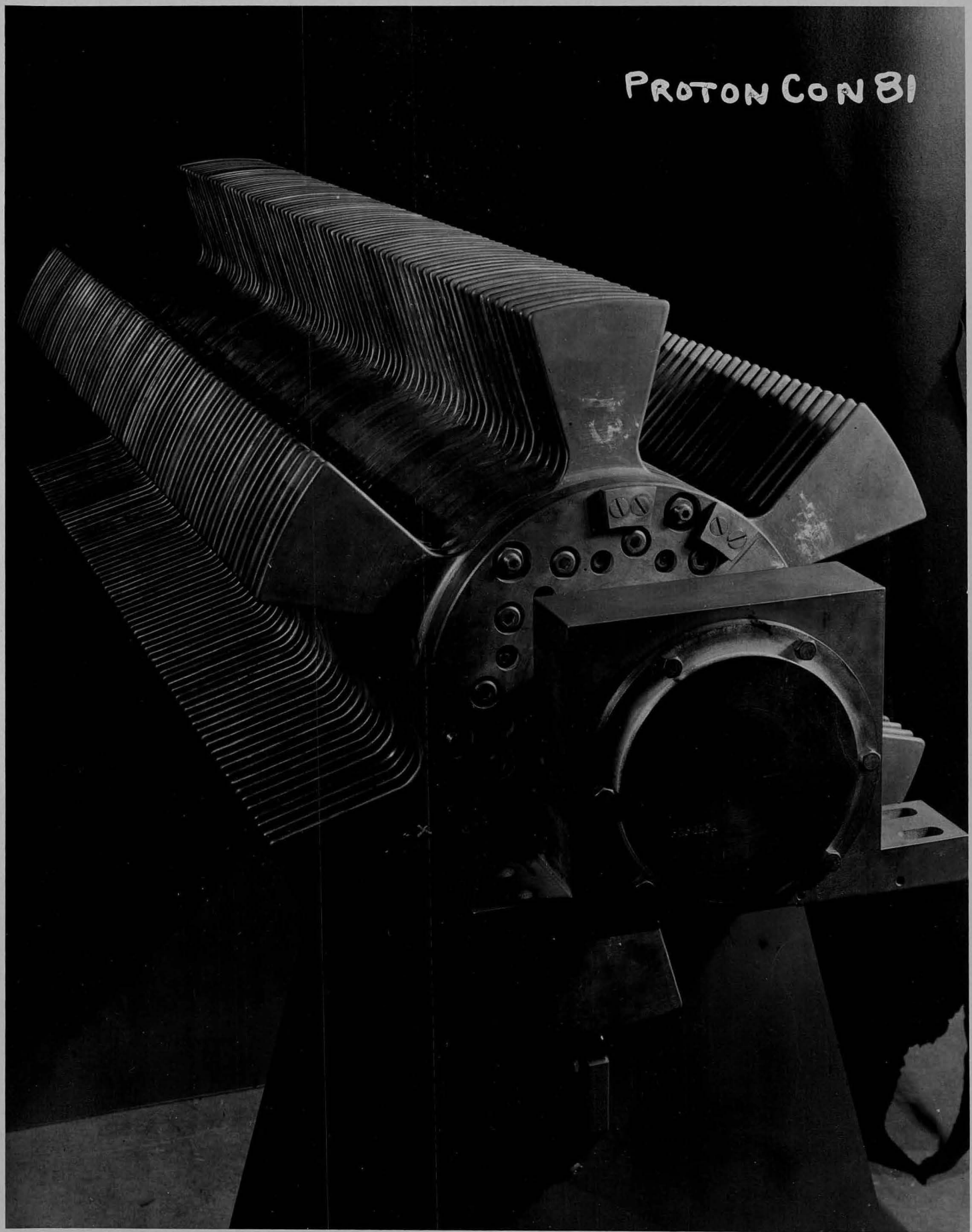

KODAK—GALLERY OZ-120


PROTON CON 85

2. Synchrotron

Marvin Martin

During the past quarter, the magnetic measuring program was completed and a considerable period was spent searching for a Mev betatron beam without success. Various experiments were performed in an attempt to determine the reason for this failure, and three possible causes discovered:

(1) A really satisfactory vacuum was never obtained although operating experience with other betatrons indicated that there should have been some beam at the synchrotron operating pressure.

(2) The magnetic field adjustment was made in accordance with the theoretical requirements and was designed to eliminate azimuthal variations of low harmonic order relative to the frequence of revolution. According to the theory, the effect of variations of a high harmonic order should be greatly attenuated and the correction of these errors was not done. Since errors in magnetic field of $\pm$ 100% of the field at injection are encountered, it is possible that the assumptions which permit these variations to exist are not valid and it is planned to reduce all magnetic field variations to approximately 10% of the injection field.

(3) On dis-assembly of the machine, it was found that an insulating varnish had been deposited on part of the surface of the conducting foil inside the vacuum chamber. It is very probable that this varnish could support a static charge which would result in the loss of the beam after a few revolutions. This theory is supported by the observation that after a short stand-by period, the first pulse of electrons to a probe 315° from the injector was much larger than subsequent pulses.

Numerous experiments were performed using a current collecting probe as a monitor and adjusting compensating coils to make the electron orbit follow the vacuum chamber. Retractable vanes were placed at approximately 45° intervals around the orbit, and the vane radius for maximum attenuation of the electron current was observed in making the adjustments. ~~It was found that~~ the orbit could be circularized with considerable accuracy by this method. The correcting coils which were available for use, however, were limited to the correction of variations having a low frequency. In order to eliminate the high frequency field variations, it will be necessary to install a large number of coils, each covering a small portion of the orbit.

Observations of the electrons during their first revolution were made using anthracene mounted in the end of a lucite rod which projected into the vacuum chamber. A photomultiplier tube adjacent to the outer end of the lucite rod was used to observe any photons generated in the anthracene by electron bombardment. This device proved to be a very sensitive detector, and its time resolution could be made very short. Most of the attempt to locate a betatron beam were made with the output from this detector displayed on an oscilloscope using a triggered sweep. Had any betatron beam existed, this device should have given a second pulse at the time the orbit collapsed into the detector.

The machine is being re-assembled with a sufficient number of compensating coils located above and below the pole tips to permit complete compensation of the field variation. The quartz doughnut will also be used to insure that a good vacuum is obtained and to provide a surface on which a satisfactory semi-conductor can be

placed. These steps should correct all known difficulties with the machine.

Some experimental work is also being started on methods for injecting a higher voltage since all of the possible troubles become less serious at higher energies. This development work is quite promising and will be explored as a side line in case the above methods of correction do not prove adequate.